Master Thesis in Physical Oceanography

Simulating the circulation in the Mozambique Channel by use of a numerical ocean model

Ole Segtnan
May, 2006

Geophysical Institute
University of Bergen

Abstract

The circulation in the Mozambique Channel for the year 2002 has been studied through model results from the Regional Oceanic Modeling System (ROMS). The model has been run with both adaptive boundary conditions and values at the open boundaries fixed to climatology.

Modeled anticyclonic eddies are generated at the northern tip of Madagascar. The migration of these eddies is mostly dependent on the background flow and to a less extend eddies' self induced motion. When conditions at the open boundaries are fixed to climatology the boundaries strongly constrain the background flow, by reflections of the flow at the southern open boundary. With boundary values fixed to climatology the modeled mean volume transport in the upper 500 m depth through the Mozambique Channel for the simulated year 2002, at 17 °S is 1.7 Sv northward, while when adaptive boundary conditions are used, the modeled mean volume transport is -3.1 Sv, which is in agreement with observations.

It is found that modeled eddies north of Madagascar are generated mainly by baroclinic instability at an approximately 15 days period. This is not seen in satellite observations and is most likely due to too strong density stratification. In both runs formation of anticyclones at a 50 days period also occur, probably related to barotropic instability of the South Equatorial Current. Generation of anticyclonic eddies at a 90 days period, possibly induced by westward traveling Rossby waves, are seen when values are fixed to climatology, but not when adaptive boundary conditions are applied.

Preface

Now that I have finished my master thesis, I have been studying the ocean for three years. During this time I have realized that the "deep blue" is just too big and too complex for the human brain to fully understand (at least for mine). The equations that describe the motion of the sea looks very simple, but when we for some reason try to solve them, it ends up in frustration. And if we are able to derive something, it is based on a set of clever tricks, so in the end it is impossible to relate it to a physical process. Still, it is peculiar how old fashion mathematics can be used to describe what's going on in the ocean. And further, allthough we don't really understand how, it seems as if the equations form part of a large scale balance. For example, it is necessary to transport heat away from the equator, and yes, according to abstract vortex dynamics, that is what we can predict happens. Based on these "coincidences", one can assume that nature is in a balance that all living creatures on the earth enjoy. Unfortunately, it is possible that the balance is threatened by environmental changes caused by humans. Changes that do not only affect the equations.

Well, that is pretty much what students at the geophysical institute are taught (before we start a career in an oil company). I will like to say thank you to the people at Geofysen for this knowledge, and for a great time.

In the work with this thesis I have received help from almost everyone at the institute, thanks to all. Especially thanks to my supervisor Professor Tor Gammelsrød for his time and superb guidance, Paul Budgell for running the model and for lots of help with all the numeric stuff, and to Kristin Richter, Kristin Rygg, Tarjei Breiteig, Frank Gaardsted and Morten Borgen for useful comments and ideas. Thanks to Frode Vikebø, for his software support. Also thanks to the Good Lord for making the ocean so interesting to study.

Contents

1 Introduction

1.1 Background

The ocean between Mozambique and the west coast of Madagascar is known as the Mozambique Channel (Fig. 1). With the coastal oceans of South-eastern Africa the Mozambique Channel forms part of what may be considered to be the greater Agulhas Current circulation. The Agulhas Current works as an interconnection between the warm Indian Ocean and the colder Atlantic Ocean by leaking water into the Atlantic Ocean, via so called Agulhas Rings (Fig. 1). This results in an inter oceanic exchange

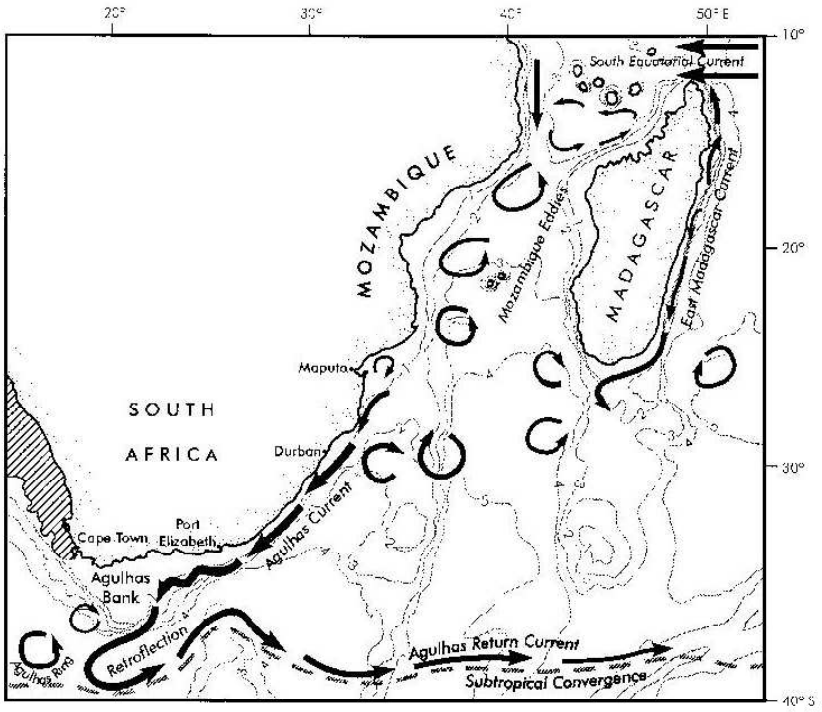

Figure 1: *The major circulation features in the Agulhas region after Lutjeharms (2005).*

of water masses, which again is of importance to the global conveyor belt (Gordon, 1986). Model studies have shown that the meridional overturning circulation of the Atlantic weakens (strengthens) with decreasing (increasing) Agulhas leakage. Within a few decades the signal propagates to the polar North Atlantic (Weijer et al., 2002). Insight of the oceanic processes in the Agulhas region can therefore give a better understanding of the climate on a global scale. In this aspect it is necessary to understand the importance of the sources of the Agulhas Current.

The Agulhas Current is supplied with water from two different sources; the South Equatorial Current (SEC) and recirculation in a South-West Indian Ocean subgyre

(Stramma and Lutjeharms, 1997). The focus of this thesis will be on how SEC feeds the Agulhas current via the circulation in the Mozambique Channel.

Previously it was thought that SEC acted as a source for two western boundary currents - the East Madagascar Current and the Mozambique Current. The Mozambique Current was believed to flow southward along the Mozambique coastline. These two western boundary currents would then have a confluence somewhere off South Africa to form the Agulhas Current.

It has been shown that there is no intense western boundary current along the east coast of Mozambique (Ridderinkokhof et al., 2001). However, the average surface drift along the eastern shelf of Mozambique is directed polewards (e.g. Sætre, 1985).
The variability of the western side of the channel is very high, but low in the eastern. This is supported by an analysis of ships drifting (Lutjeharms et al., 2000a), altimetric observations (Lutjeharms et al., 2000b) and also by numerical models (Biastoch and Krauss, 1999). These results agree with the concept of a train of eddies moving poleward through the western part of the channel. From model results (Biastoch and Krauss, 1999) and also satellite observations (Schouten et al., 2003), it has been demonstrated that anticyclonic eddies are generated at the northern tip of Madagascar. As these relatively wide and deep anticyclones migrate southward through the channel, they represent an important transport of water to the Agulhas Current. Anticyclonic eddies in the Mozambique Channel will therefore influence the Agulhas Current's behavior indirectly and can be considered to constitute an inherent part of the greater Agulhas system.
For a detailed description see Lutjeharms (2005).

1.2 Objectives

The main objective of this thesis is to contribute to a better understanding of the ocean circulation in the Mozambique Channel. Results from the Regional Oceanic Modeling System will be validated against observations, to see if the model gives a realistic description of the circulation in the Mozambique Channel.

To validate the model-results, I will present observed sea surface temperature and sea surface elevations from satellites from 2002, and drifter data from 2000. Results from moored current measurements (Ridderinkhof et al., 2003) and lowered ADCP observations (Schouten et al., 2002), found in previous published papers, will also be used. The validation will cover both the large scale picture and the mesoscale circulation. The focus will be on the anticyclonic eddies generated at the northern tip of Madagascar, their formation, hydrography and migration.

The thesis is constituted as follows: In Chapter 2 the numerical model and the methods for collecting observed data are described. Modeled and observed results are presented in Chapter 3. A discussion of the results is given in Chapter 4. Finally, the clarified points are summarized in Chapter 5.
Theory for understanding some of the basic concepts in eddy dynamics is presented in the discussion (Chapter 4) and in the appendices (A-D).

2 Model and data

2.1 Model

In this master thesis I have worked with results from the Regional Oceanic Modeling System (ROMS). A description of the development is found in Song and Haidvogel (1996). The model was run by Paul Budgell at the Institute of Marine Research in Bergen, for the year 2002. Two different runs have been performed with different conditions at the open boundaries. These are described in Section 2.1.3. The model covers the Mozambique Channel and the region around Madagascar. Figure 2 shows the model domain. All model outputs are given as daily means.

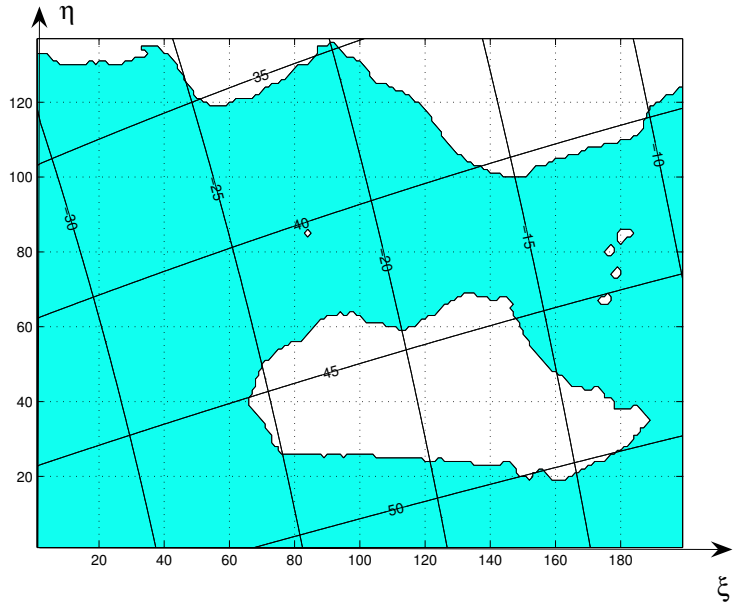

Figure 2: *Model domain: ξ and η denotes the axes of model grid points. Latitudes and longitudes are drawn.*

2.1.1 Coordinates

Horizontal coordinates:

The horizontal axes are denoted ξ and η (Fig. 2). To keep high resolution in the entire model domain, resolution is equal everywhere. It then follows that ξ and η can not be east-north coordinates. However, because the domain is so limited in size, the north and east axis are considered to be straight lines. The north and east component of ξ and η are then found by means of the angle between the north axis and the ξ axis. From Figure 2 it is seen that this angle is approximately 18 °.

To properly model mesoscale motion it is necessary to resolve not only the length scale of the mesoscale features, but also the length scale of the processes responsible for their growth and decay, i.e. the internal Rossby radius of deformation (Roed and Fossum, 2002). The horizontal resolution is 10 km everywhere which is normally less than the internal Rossby radius.

Vertical coordinates:

In the vertical, ROMS uses stretched, terrain-following coordinates. Terrain-following coordinates (σ) are calculated as follows:

$$\sigma = \frac{z - \zeta}{H + \zeta}, \qquad , \tag{1}$$

where ζ is the surface elevation, z is the altitude depth and H is the equilibrium depth. σ goes from -1 (bottom) to 0 (surface), and is divided into 30 layers, where layer number 30 is the surface layer (referred to as σ layer 30).

For better resolution in the areas of interest, such as at the thermocline and at the bottom boundary layers, stretched coordinates are introduced. z is then calculated as:

$$z = H_c \cdot \sigma + (H - H_c) \cdot Sc \, , \tag{2}$$

where S_c is the stretched coordinates, one for each σ layer. The critical depth, i.e. the minimum depth in the region is represented by H_c and is equal to 10 m.

2.1.2 Forcing

Atmospheric forcing is obtained from the NCEP/NCAR reanalysis data (Kalnay et al., 1996). Daily mean wind stress, and latent, sensible, downward shortwave radiate and net long wave radiative heat fluxes are applied as surface forcing.

2.1.3 Boundary conditions

With high spatial resolution and finite computer resources the model coverage must be of limited size and therefore enclosed by both solid and open boundaries. Coastal boundaries can be specified as a finite-discretized grid via land/sea masking. At the open boundaries the model has been run with two different sets of boundary conditions:

(1) Boundary values fixed to climatology
(2) Adaptive boundary conditions

(1) Boundary values fixed to climatology

In the first model run (model run 1) the values at the open boundaries are fixed to climatology. Values at the open boundaries are given as linearized, monthly means of the MICOM model. In the Mozambique Channel area MICOM has a resolution of 300 km and are fitted to the model grid size by linear interpolation. In addition to the boundary values from MICOM, daily means of Topex global ocean tidal data assimilation are added.
A linear relaxation buffer zone of 10 grid points are used to achieve continuity with the interior solution.

(2) Adaptive boundary conditions

A second run (model run 2) was performed with adaptive open boundary conditions. For a detailed description see Marchesiello et al. (2001). Adaptive conditions are used when the flow through the open boundary may be either inwards or outwards. When propagation is outwards the idea is to use radiation conditions to allow disturbances out of the model domain. For inflow, external values at the boundaries are used to force the interior solution.

The radiation condition for a prognostic model variable Φ is :

$$\frac{\partial \Phi}{\partial t} + c_x \cdot \frac{\partial \Phi}{\partial x} + c_y \cdot \frac{\partial \Phi}{\partial y} = 0 \tag{3}$$

where (x, y) are the normal and tangential directions to the boundary, respectively. The phase speeds in normal and tangential directions are given by c_x and c_y. They are derived from Equation (3) and calculated from the Φ field surrounding the boundary point as follows:

$$c_x = -\frac{\partial \Phi}{\partial t} \cdot \frac{\frac{\partial \Phi}{\partial x}}{(\frac{\partial \Phi}{\partial x})^2 + (\frac{\partial \Phi}{\partial y})^2} \ , \tag{4}$$

$$c_y = -\frac{\partial \Phi}{\partial t} \cdot \frac{\frac{\partial \Phi}{\partial y}}{(\frac{\partial \Phi}{\partial x})^2 + (\frac{\partial \Phi}{\partial y})^2} \ , \tag{5}$$

The radiation condition is used independently for all dimensional prognostic variables.

When the phase speed normal to the boundary is negative (inward propagation), external data are used at the open boundary. Since the model solution cannot be perfectly consistent with the external data it is expected that after a period with outward propagation the predicted values at the boundary have evolved to be different from the external data values. This can cause problems for inflow conditions. To overcome this

problem, an additional nudging term is added to the radiation equation (3):

$$\frac{\partial \Phi}{\partial t} + c_x \cdot \frac{\partial \Phi}{\partial x} + c_y \cdot \frac{\partial \Phi}{\partial y} = -\frac{1}{\tau} \cdot (\Phi - \Phi_{ext}) \; , \tag{6}$$

with

$$\begin{aligned} \tau &= \tau_{out} \qquad \text{if} \qquad c_x > 0 \; , \\ \tau &= \tau_{in} \qquad \text{and} \qquad c_x = c_y = 0 \qquad \text{if} \qquad c_x < 0 \; , \end{aligned}$$

The external data is represented by Φ_{ext}, and τ is the time scale for nudging, with $\tau_{out} \gg \tau_{in}$. Equation (6) is applied at the grid points near the open boundary, the so called nudging layer. τ varies smoothly from τ_{in} to infinity within the nudging layer.

In model run 2 the nudging layer consists of 10 grid points, τ_{in} = 5 days and τ_{out} = 100 days. Over the nudging layer $\frac{1}{\tau}$ goes like a cosine function from $\frac{1}{5 \cdot 84600s}$ to 0. External boundary data are from MICOM and Topex (same conditions as in model run 1).

2.1.4 Initial values and spin-up

Model run 1 has a spin-up period of one year (2001). Initial values are obtained from a previous model run which simulates 2004 for the same model domain, forcing and boundary conditions (fixed to climatology). For the 2004 run initial conditions are from MICOM and NCEP/NCAR, and the spin up period is one year (2003). Also model run 2 has a spin up period of one year (2001), where initial values are obtained from model run 1.

2.2 Data

2.2.1 Satellite data

Sea surface elevations:

Sea level anomalies from satellites are available online at ftp://ftp.cls.fr/pub/oceano/AVISO/. They are given as weekly, merged (from several satellites) means, with a resolution of $\frac{1}{3}^\circ \times \frac{1}{3}^\circ$. Sea level anomalies are deviations from the average of all observations made. (Both time mean and global spatial averages).

Sea surface temperature:

Sea surface temperature from satellites are available online at http://www.remss.com/. They are given as daily, merged means, with a resolution of $\frac{1}{4}^\circ \times \frac{1}{4}^\circ$. The sea surface temperature is updated several times per day, which ensures reliable results.

2.2.2 Floats

During Cruise 64PE156 with RV Pelagia in the Mozambique Channel March 20 - April 13, 2000, eight ARGOS drifters were deployed. The drifters used were standard spherical WOCE/TOGA mixed layer drifters (diameter 30 cm), fitted with a holey sock drogue at 15 m. The drogues have a length of 7 m, and a diameter of 1 m (Ridderinkhof et al., 2001). The positions of the drifters are given every fourth to sixth hour by satellite tracking. Only data from three of the eight drifters that are available are used in this thesis. I have chosen to focus on anticyclonic eddies in the Mozambique Channel and six of the drifters are either deployed too far south or do not follow the tracks of an eddy.

3 Results

3.1 Sea surface temperature

Figure 3 shows modeled (run 1 and run 2) and observed (satellites) mean sea surface temperature in the Mozambique Channel for January 2002. Meridional temperature distribution is similar for model and satellite results. The temperatures range from 25 °C to 29 °C with a decrease in temperature gradient at approximately 24 °S.
South of 20 °S both run 1 and run 2 show an eastward increase in temperature. In the satellite observation it is opposite, with warmest water in the western part of the channel.

The modeled and observed mean sea surface temperatures in the Mozambique Channel for August 2002 are shown in Figure 4. Observed temperatures lie in the range 20 °C - 26 °C. For model run 1 and run 2 they go from 20 °C to 25 °C. At approximately 22 °S there is an decrease in temperature gradient, in observations as well as in the model results.
For run 1 temperatures are lower on the western side of the channel, near the coast of Mozambique, than farther east. Satellite observations and run 2 show higher values near the coast of Mozambique and the west coast of Madagascar, than in the middle of the channel.

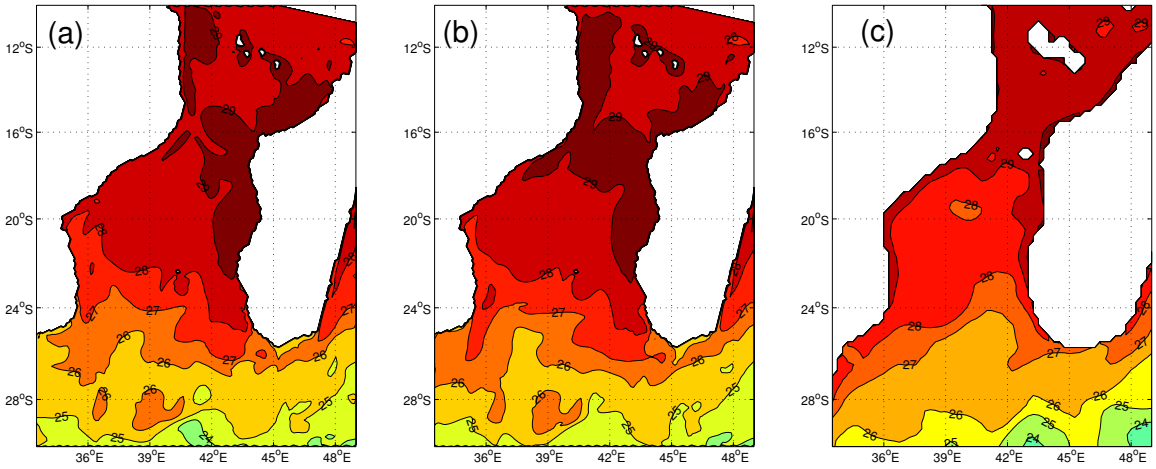

Figure 3: *Mean sea surface temperature in the Mozambique Channel January 2002: (a) model run 1, (b) model run 2, (c) satellite observations.*

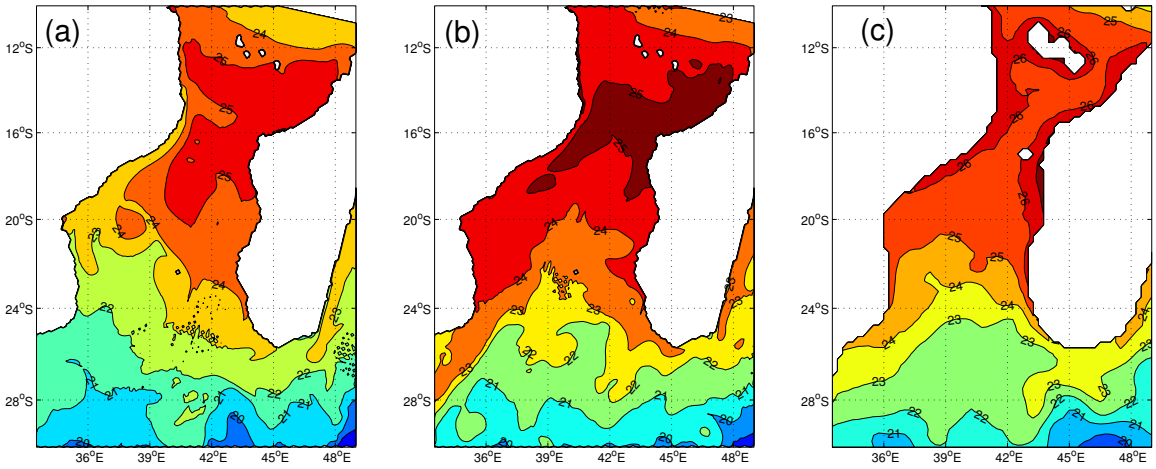

Figure 4: *Mean sea surface temperature in the Mozambique Channel August 2002: (a) model run 1, (b) model run 2, (c) satellite observations.*

.

3.2 Sea surface height

The modeled and observed mean sea surface elevation in the Mozambique Channel for January 2002 are presented in Figure 5. To better study local variations within the channel, the average spatial surface elevation is subtracted. All results show great variability for the sea surface elevation in the Mozambique Channel. In this thesis areas of increased and depressed sea surface are referred to as high pressures and depressions, respectively.

In run 1 high pressures are located north of 22 °S and south of 27 °S, with four high pressures situated north of 22 °S. Their amplitudes, which is the maximum anomaly of a high pressure or a depression, range from 10 to 25 cm. For the three northernmost high pressures, the amplitudes are decreasing towards the equator. The horizontal scale is approximately 200 km.
In the area between 19 °S and 27 °S, several depressions are found. Their amplitudes lie between -15 and -20 cm and they have a horizontal scale of the same order as the high pressures.
In run 2, three high pressures are located north of 21 °S, at roughly the same locations as those in model run 1. The horizontal scales are near 250 km, with amplitudes from 20 to 25 cm. Compared to run 1, the amplitudes are 5 cm higher for the two high pressures closest to the equator. Areas of depressed sea level are found in the region from 19 °S to 27 °S, the same location as for run 1. Amplitudes of the depressions go from -15 to -25 cm.
Unlike the model results, satellite images of the sea surface elevation show that in January 2002, high pressures are also found between 22 °S and 27 °S. High pressures are mainly located on the western side of the channel, near the coast of Mozambique. The horizontal scale and the amplitudes increase away from the equator. A high pressure at 22 °S 38 °E has an amplitude of 35 cm and horizontal scale of approximately 300 km. Depressions have a similar horizontal scale, and amplitudes from 20 to 30 cm.

Figure 6 shows modeled and observed mean sea surface heights in the Mozambique Channel for August 2002. In run 1, high pressures are still only present in the northern and southern part of the channel, in the regions south of 27 °S and north of 21 °S. In the area between, four depressions are located. The amplitudes of the high pressures in the northern part of the channel are smaller than in January, with a maximum value of 15 cm.
Results from run 2 show three high pressures along the western side of the channel, near the coast of Mozambique, at 20 °S, 23 °S and 30 °S. The high pressure at 23 °S has an amplitude of 40 cm. West of the two high pressures at 20 °S and 23 °S, along the coast of Mozambique, the sea surface is depressed. Values as low as -35 cm are seen. Depressions are also found in the southern part of the channel, from 28 °S to 22 °S.
Satellite observations show that several high pressures are located along the coast of Mozambique at all latitudes. Amplitudes are smaller than what was seen in January with a maximum value of 20 cm. Depressions have a random distribution. Their horizontal scales are larger compared to January. Also the amplitude of depressions have increased, now with values of -40 cm.

.

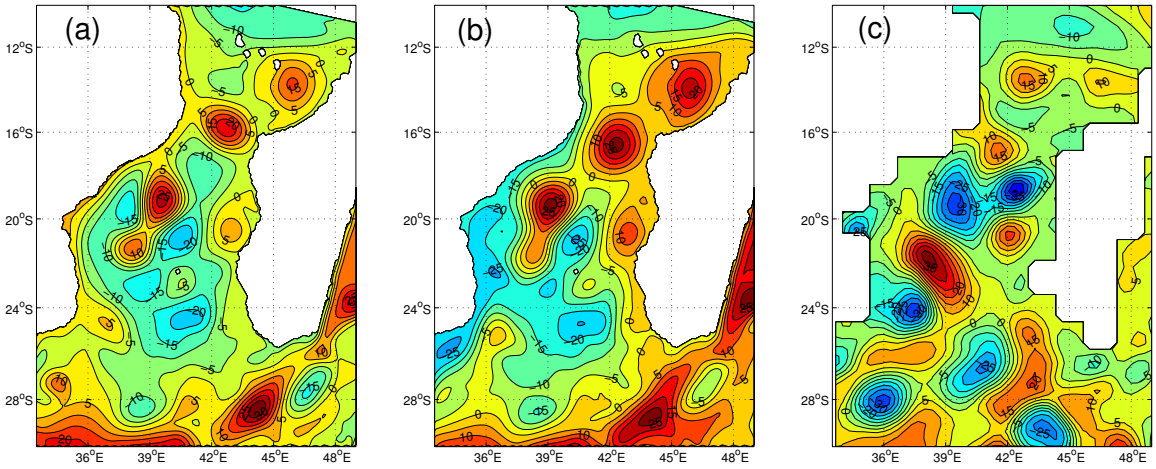

Figure 5: *Mean sea surface height in the Mozambique Channel January 2002: (a) model run 1, (b) model run 2, (c) satellite observations.*

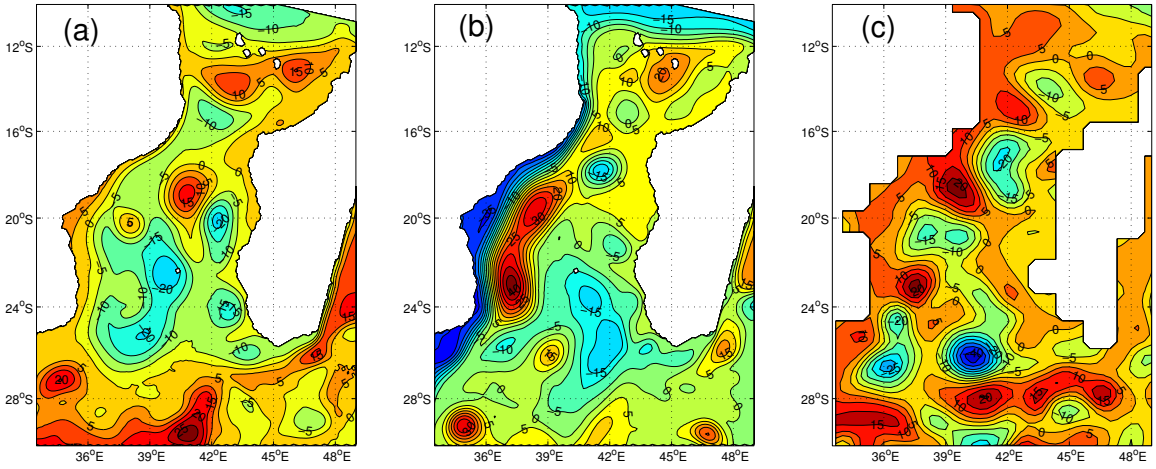

Figure 6: *Mean sea surface height in the Mozambique Channel August 2002: (a) model run 1, (b) model run 2, (c) satellite observations.*

3.3 Transport estimates

Modeled volume transports have been calculated through a vertical cross section at 17 °S (Section AB, Figure 7). The section covers the upper 500 m layer. It goes from the coast of Mozambique to the west coast of Madagascar, and has been separated into a western and an eastern part at 42 °E. In Figure 8 a) - d), the modeled transports are shown as net volume transports through section AB, and the volume transports separated into the contributions from the western and the eastern part of the section.

Modeled volume transport from run 1 shows that transports vary between northward and southward directions through both the western and eastern part of the section

(Fig. 8 c)). The magnitude of the transport has maximum value in austral summer (Fig. 8 a)). Northward transports are seen in the first 150 days, after this period the transports are varying between northward and southward. Mean transport for 2002 is 1.7 Sv northwards (1 Sv = 10^6 $\frac{\mathrm{m}^3}{\mathrm{s}}$).
In run 2 the flow through the western part of the section is mainly southwards, while the flow through the eastern is in general directed northwards. In the first 200 model days the net transport is mainly southwards. After 200 days the net volume transport changes between northward and southward direction. Mean transport for 2002 is -3.1 Sv.

During 2000 and parts of 2001, Ridderinkhof et al. (2003) calculated volume transports through the cross section at 17 °S (Section AB), by use of current measurements (CM-RCM 8). The array of moorings contains 7 instruments. The transport has been divided into a western and eastern contribution at 42 °E. Figure 9 shows the volume transports in the upper 500 m layer divided into a western and eastern contribution at 42 °E. Through the western section the transport is almost entirely southwards. For the eastern mainly northwards, but also with some southward transports. High southward volume transport through the western section always correspond to high northward transports through the eastern section. 4 strong pulses are seen for 2000/2001, but also weaker signals are present. Ridderinkhof et al. (2003) found the observed mean transport through the whole section for the upper 500 m depth in 2000/2001 to be -7.2 Sv.

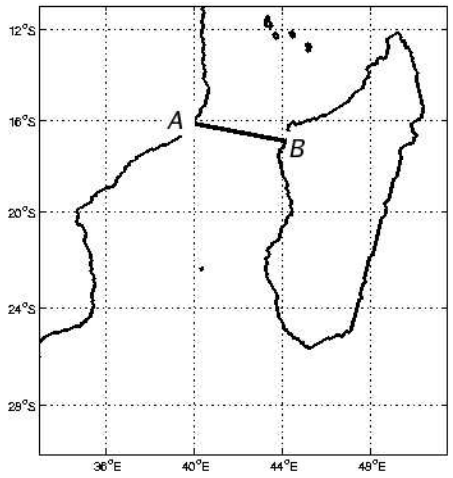

Figure 7: *Section AB: Vertical cross section through the Mozambique Channel at* 17 °S

RUN 1: RUN 2:

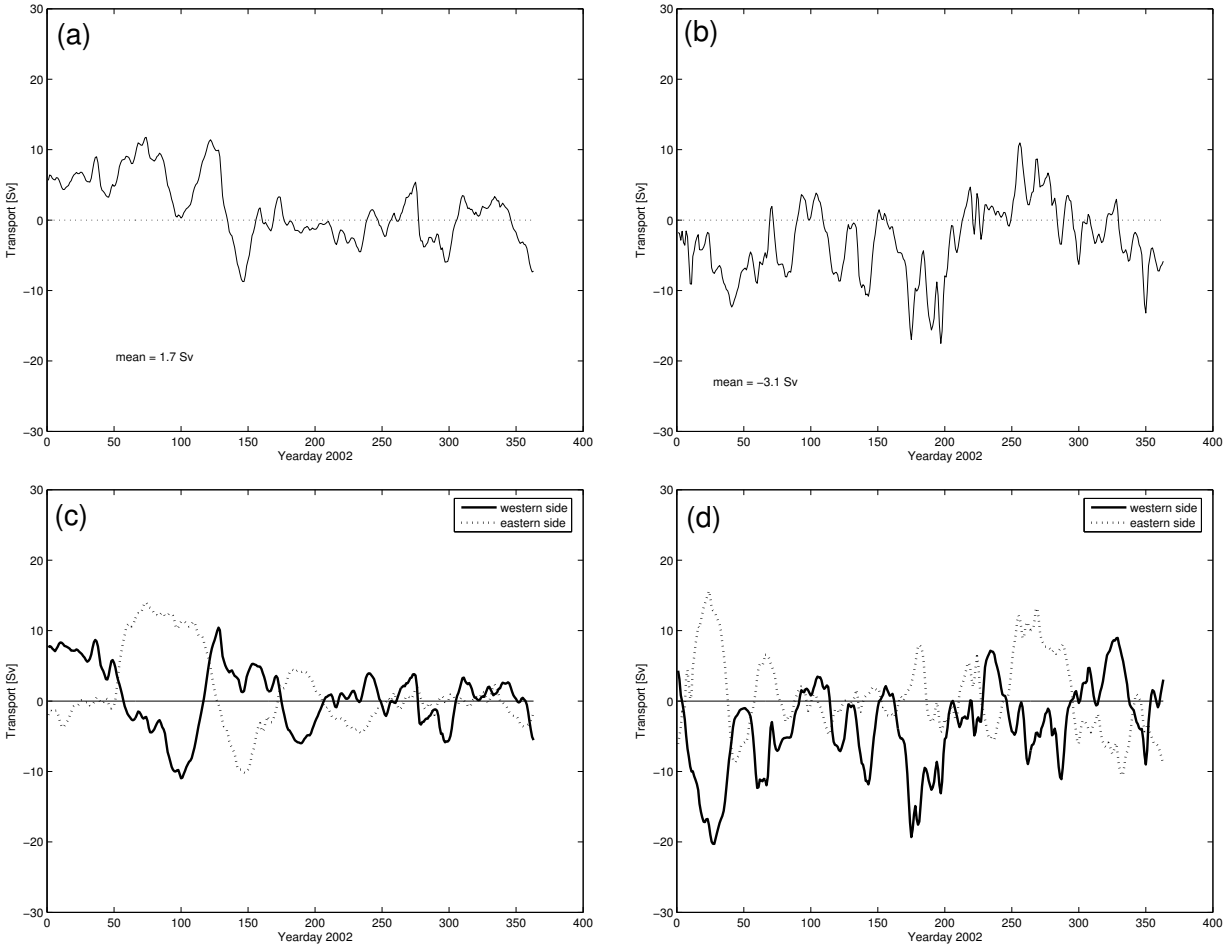

Figure 8: *Modeled volume transports [Sv] for the upper 500 m depth through section AB (Fig. 7) the year 2002. a) and c) show results from run 1, b) and d) from run 2. a) and b) show the net transport through the entire section, c) and d) show the transport divided into one contribution from the western side (solid lines) and one from the eastern (dashed lines). Positive (negative) values denote northward (southward) velocities.*

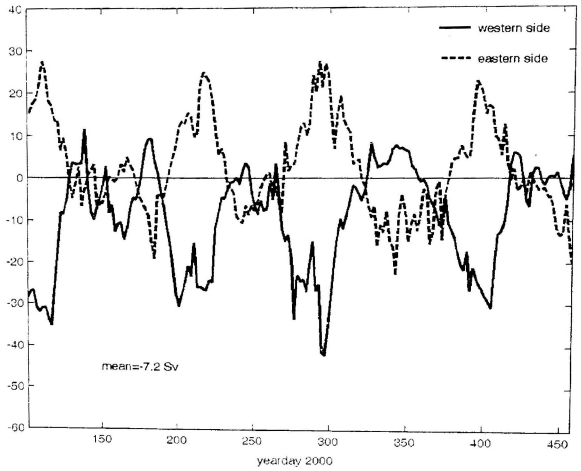

Figure 9: *Observed volume transport [Sv] for the upper 500 m depth through section AB (Fig. 7) for 2000/2001. The solid lines shows the transport through the western side, the dashed line through the eastern side. Positive (negative) values denote northward (southward) velocities. The figure is taken from Ridderinkhof et al. (2003)*

3.4 Vertical structure of anticyclonic eddies

The vertical structure of modeled and observed anticyclonic eddies in the Mozambique Channel is presented in this section. Modeled anticyclones are identified from plots of velocity vectors in the surface layer.

Figure 10 and 11 show vertical sections of temperature, salinity, meridional velocity, density and surface elevation for two modeled anticyclonic eddies in the Mozambique Channel, from run 1 (eddy 1) and run 2 (eddy 2) respectively. All sections are taken along the eddies' zonal diameter. The spatial average of the surface elevation in the channel is subtracted. The two modeled eddies investigated are located at 21 °S near the coast of Mozambique.

In the Mozambique Channel the modeled density contours mainly follow temperature rather than salinity. In the upper 2500 m, the temperature generally varies with more than 20 °C, while salinity lies in the range 34.5 - 35.5. (Fig. 10 and 11). For the two anticyclonic eddies investigated, the density increases away from the eddy center, causing modeled anticyclonic eddies in the Mozambique Channel to have a baroclinic velocity component as well as the barotropic.

In simulation 1 (eddy 1) strongest horizontal density variations are seen down to 300 m depth (Fig. 10). In the upper 300 m depth variations in the swirl velocity are also strong. Near the surface velocities are roughly 70 $\frac{\text{cm}}{\text{s}}$, at 300 m depth they are approximately 20 $\frac{\text{cm}}{\text{s}}$.
In the upper 400 m depth velocities are higher on the eastern side, below they are higher on the western. The eddy reaches down to approximately 1000 m with velocities of 5 $\frac{\text{cm}}{\text{s}}$.
The maximum sea surface elevation of eddy 1 is 25 cm.

In contrast to eddy 1, eddy 2 is situated so that it intersects with the coast (Fig. 11). The strongest horizontal density gradients of eddy 2 are found in the upper 300 m layer, but also near the shelf there are horizontal density gradients in all depth levels. The greatest vertical variations in swirl velocity are also found in the upper 300 m depth. On the eastern side of the eddy velocities go from 120 $\frac{\text{cm}}{\text{s}}$ near the surface down to 60 $\frac{\text{cm}}{\text{s}}$ at 300 m depth. From 300 m depth the velocity gradient is weaker. Speeds up to 20 $\frac{\text{cm}}{\text{s}}$ are seen down to nearly 3000 depth. On the western side of the eddy, on the slope, vertical velocity gradients ($\frac{\partial \text{u}}{\partial \text{z}}$) are stronger than on the eastern side. From the surface and down to almost 2000 m depth, the velocity decreases gradually from 120 $\frac{\text{cm}}{\text{s}}$ southwards to 20 $\frac{\text{cm}}{\text{s}}$ southwards.
The maximum surface elevation of eddy 2 is 70 cm.

Meridional velocity through the zonal diameter of eddy 1 and eddy 2 are shown in Figure 12 and 13 at four different depths. The figures show that the maximum swirl velocity is located halfway between the eddy center and the eddy edge, i.e. if r is the distance from the eddy center, the maximum swirl velocity is found near $r = \frac{r_0}{2}$, where r_0 is the eddy radius.

Results from run 1 (eddy 1) show northward velocities west of the anticyclonic eddy, near the coast of Mozambique (Fig. 12). This jet like feature is most dominant in the deeper layers.
In Figure 13 it is seen that on the western part of eddy 2, southward directed velocities are added to the swirl velocity.

In April 2000, three Mozambique eddies were hydrographically sampled during the first Agulhas Current Sources Experiment campaign (ACSEX 1; De Ruijter et al., 2002). Lowered Acoustic Doppler Current Profiler (LADCP) measurements of an anticyclonic eddy at 17 °S (Fig. 14) reveal the velocity field associated with this eddy (eddy 3). The LADCP can not measure velocities in the upper 150 m depth. The highest speeds are found at 150 - 200 m depth with values of 50 $\frac{\text{cm}}{\text{s}}$. The vertical velocity gradient is not as steep as for the two modeled anticyclonic eddies. From approximately 150 m depth down to nearly 1500 m depth, the swirl velocity only decreases with roughly 20 - 30 $\frac{\text{cm}}{\text{s}}$, from 50 $\frac{\text{cm}}{\text{s}}$ to 20 - 30 $\frac{\text{cm}}{\text{s}}$. Velocities as high as 10 $\frac{\text{cm}}{\text{s}}$ are seen all the way to the bottom ($\sim$ 2000 m depth).

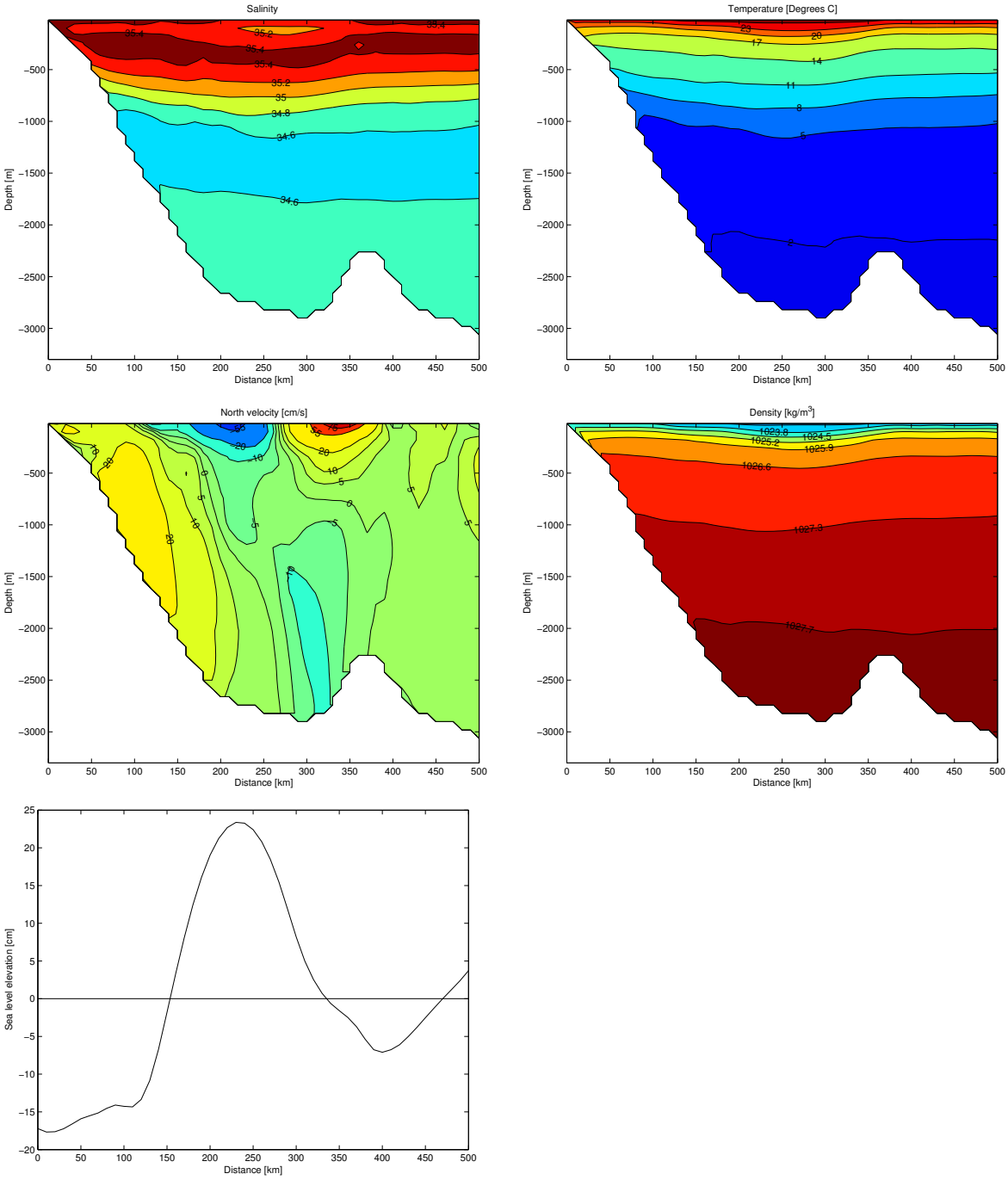

Figure 10: *Modeled salinity, temperature, velocity, density and surface elevation from run 1 through an anticyclonic eddy's diameter at* 20.6 °S 38.4 °E *model day 358 (eddy 1). Positive (negative) velocities are northwards (southwards).*

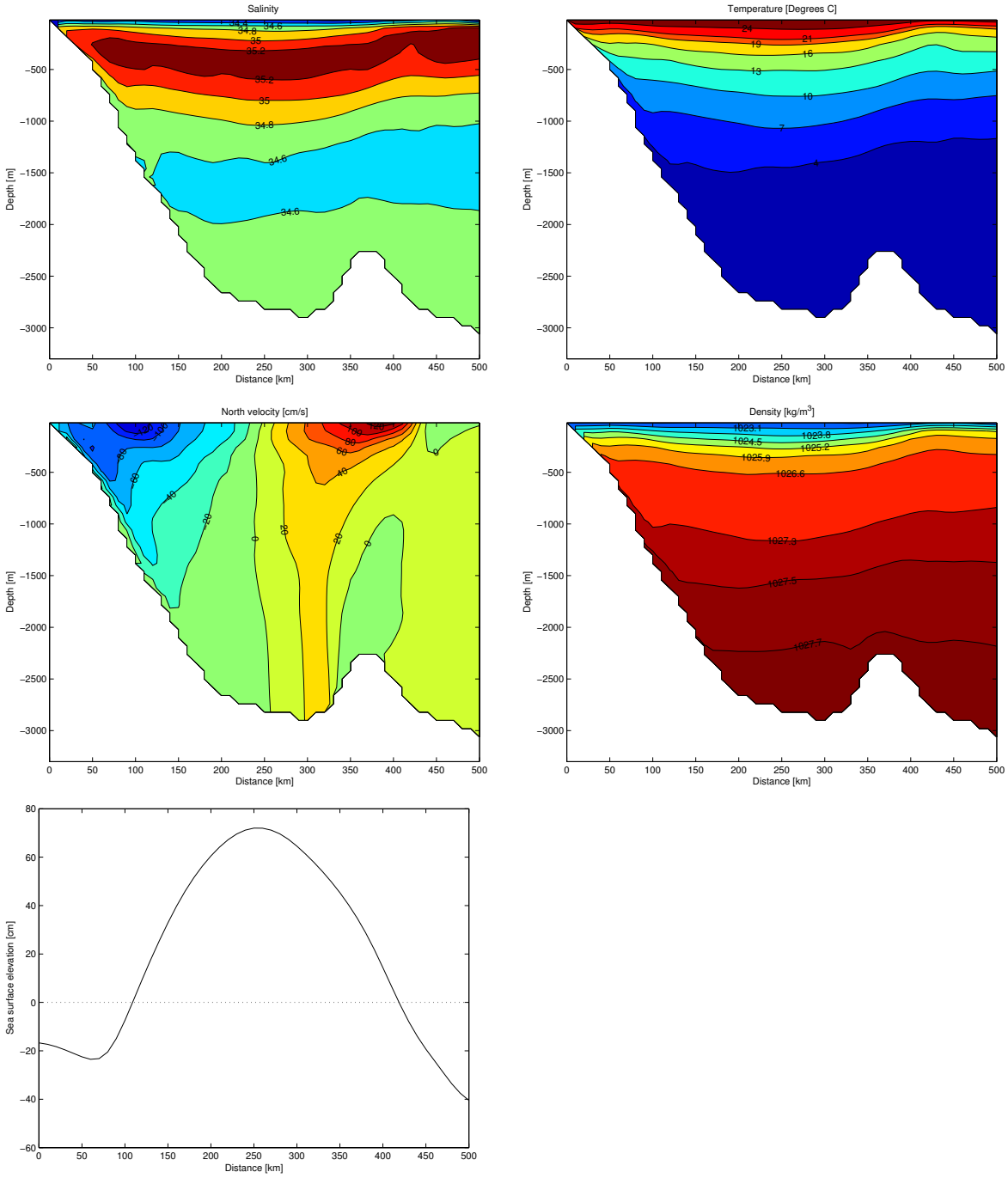

Figure 11: *Modeled salinity, temperature, velocity, density and surface elevation from run 2 through an anticyclonic eddy's diameter at* 20.6 °S 38.4 °E *model day 313 (eddy 2). Positive (negative) velocities are northwards (southwards).*

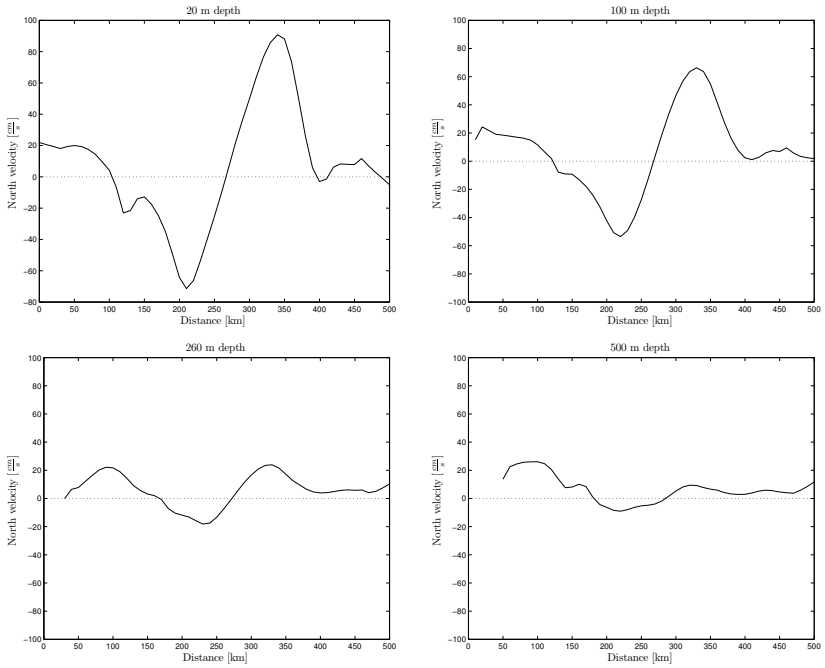

Figure 12: *Modeled meridional velocity through the zonal diameter cross section of eddy 1 at four different depths. Positive (negative) velocities are northwards (southwards).*

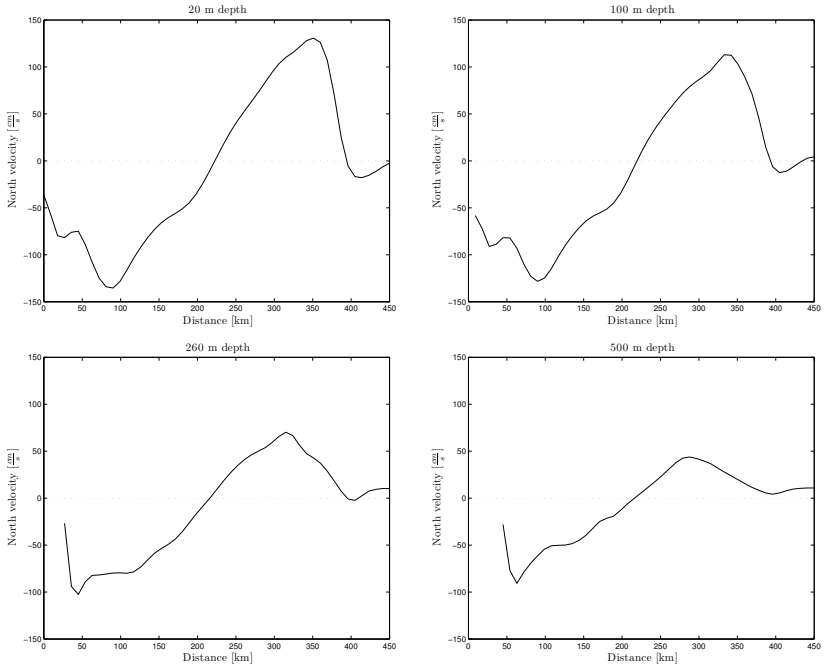

Figure 13: *Modeled meridional velocity through the zonal diameter cross section of eddy 2 at four different depths. Positive (negative) velocities are northwards (southwards).*

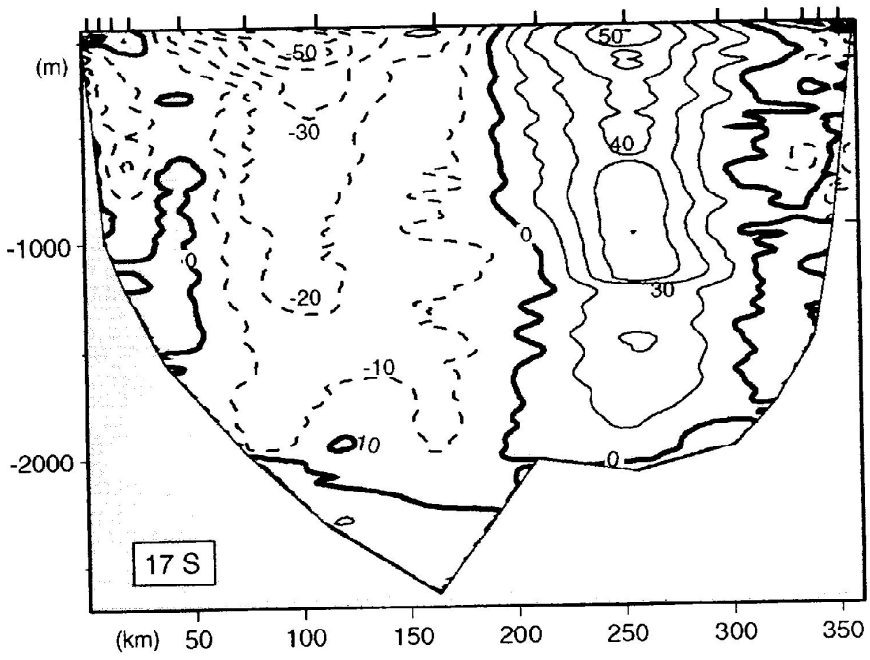

Figure 14: *Observed meridional velocity from LADCP through an eddy's zonal diameter taken in April 2000 in the Mozambique Channel near* 17 °S *(eddy 3). Positive (negative) values denote northward (southward) flow. The figure is taken from Schouten et al. (2002).*

3.5 Drifters

During Cruise 64PE156 with the Dutch ship RV Pelagia in the Mozambique Channel March 20 - April 13, 2000, eight ARGOS drifters were deployed. Data from three of them are presented in this chapter.

Figure 15 (a) shows the path of drifter 1, deployed at 17 °S 43 °E, from April 8 to September 10, 2000. At approximately 20 °S the drifter is trapped in an anticyclonic eddy located near the coast of Mozambique. Controlled by the dynamics of the anticyclonic vortex, the drifter is forced into circular motion. These three circles are drawn in Figure 15 (b) - (d) for the time periods April 18 - May 2, 2000, May 1 - May 12, 2000 and May 12 - May 27, 2000. The circle shown in figure 15 (d) is disturbed, and has a more elliptic shape.

In Table 1 the radius of the circles are listed with the corresponding average velocity of drifter 1. A clear relation between radius and velocity is not seen. With a radius of 122 km the drifter has an average velocity of 80 $\frac{\text{cm}}{\text{s}}$, while the average velocity is only 60 $\frac{\text{cm}}{\text{s}}$ when the radius is 120 km.

Figure 16 (a) - (e) show the path of drifter 2, deployed at 20 °S 39 °E, from March 30 to September 10, 2000. (a) shows the path for the entire drifting period, while (b) - (e) show the path of drifter 2 for four specific time periods. Unlike drifter 1, this drifter is trapped directly into an anticyclonic eddy. The eddy is located near the eastern coast of Mozambique and is relatively stationary near 20 °S for more than five months. The drifter follows circles with increasing size so there must be a net radial force away from the eddy center, possibly due to friction. The average orbital velocity of drifter 2 as it follows these circles is listed in Table 2.

Figure 17 shows the path of drifter 3, deployed at 24 °S 35 °E, from March 28 to May 13, 2000. The drifter is moving polewards in anticyclonic motion a short distance away from the African eastern coastline. It's average southward velocity is 10 $\frac{\text{cm}}{\text{s}}$ (8.5 $\frac{\text{km}}{\text{day}}$).

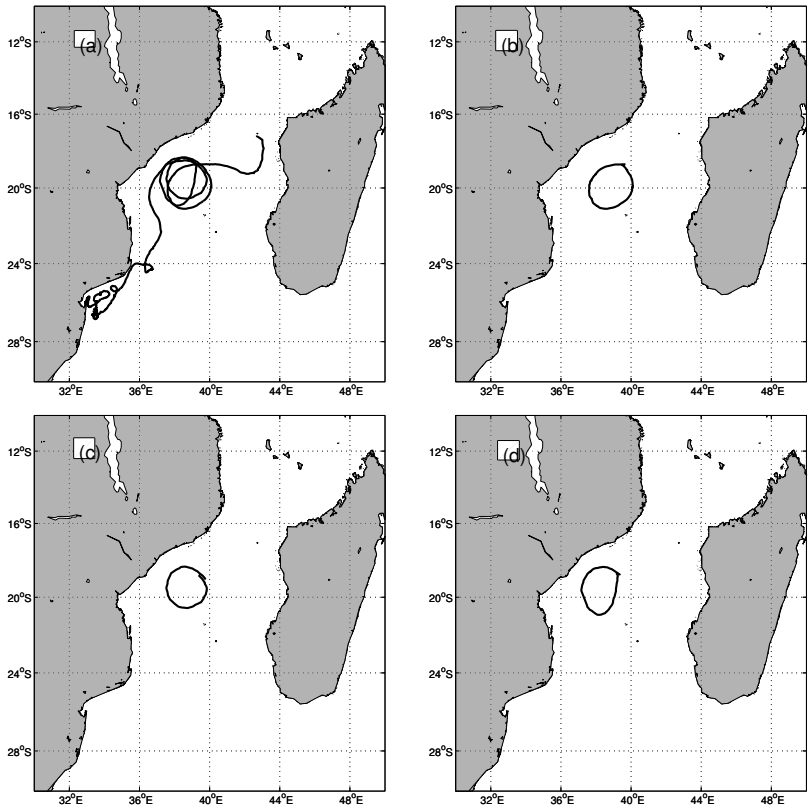

Figure 15: *Trajectories of drifter 1, deployed at* 18 °S 43 °E *April 8, 2000. (a) shows the path from April 8 - September 10, (b) April 18 - May 2, (c) May 1 - May 12 and (d) May 12 - May 27.*

Radius [km]	Orbital velocity $[\frac{\text{cm}}{\text{s}}]$	Time period (2000)
130	69	April 18 - May 2
122	80	May 1 - May 12
120	60	May 12 - May 27

Table 1: *Calculated average orbital velocity from drifter 1*

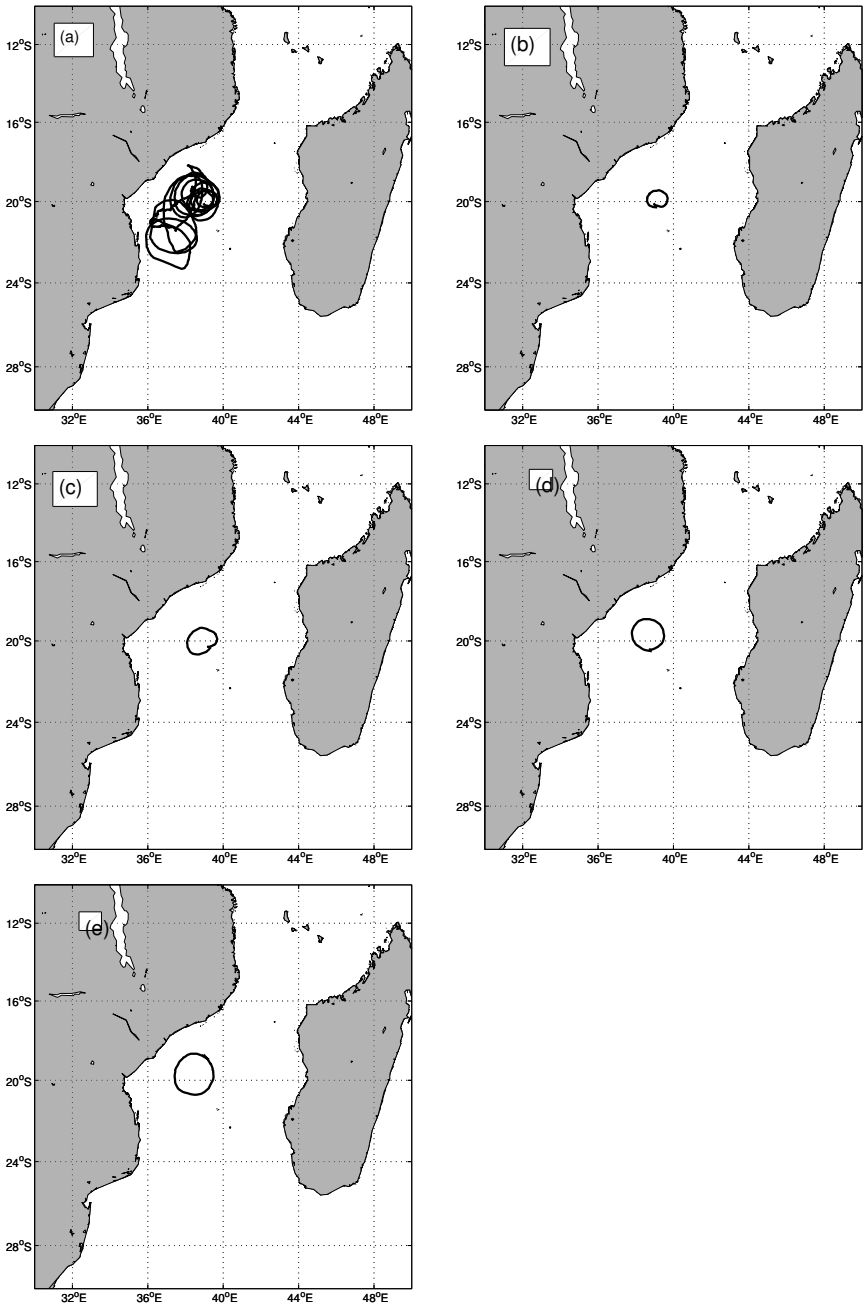

Figure 16: *Trajectories of drifter 2, deployed at* 20 °S 39 °E*, March 30. (a) shows the path from March 30, 2000 - September 9, 2000, (b) March 30, 2000 - April 6, 2000, (c) April 6, 2000 - April 13, 2000, (d) April 26, 2000 - May 4, 2000 and (e) May 7, 2000 - May 18, 2000*

Radius [km]	Orbital velocity [$\frac{\text{cm}}{\text{s}}$]	Time period
58	60	March 30, 2000 - April 6, 2000
82	85	April 6, 2000 - April 13, 2000
92	83	April 26, 2000 - May 4, 2000
110	76	May 7, 2000 - May 18, 2000

Table 2: *Calculated average orbital velocity from drifter 2*

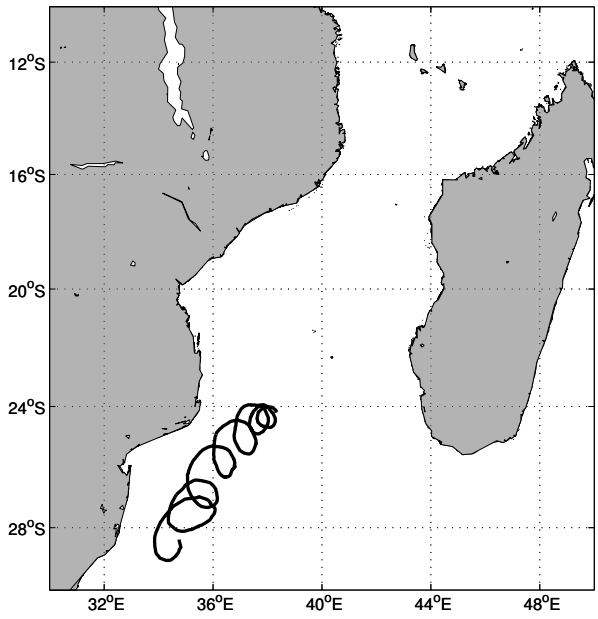

Figure 17: *Trajectories of drifter 3 deployed at* 24 °S 35 °E *from March 28, 2000 - May 13, 2000*

3.6 Eddy migration

Methods:

Since the dynamics of anticyclonic motion are related to an increased sea surface elevation (see Chapter 4), images of the sea surface heights can be used to track anticyclonic eddies in the Mozambique Channel. By monitoring high pressure locations during a time period, the pathway of anticyclonic eddies in the Mozambique Channel is revealed. Both modeled and observed eddies are tracked this way.

In this section the migration of five anticyclonic eddies is presented, two from run 1, one from run 2 and two from satellite observations. Other anticyclonic vortices follow similar pathways, thus Figure 18 - 22 give a sufficient picture of the migration of anticyclones in the Mozambique Channel.

Results run 1:

In run 1 modeled anticyclonic eddies in the Mozambique Channel are mainly formed at the northern tip of Madagascar, but anticyclones are also generated farther south, at the west coast of Madagascar near 16 °S.

Figure 18 shows modeled velocity vectors and sea surface heights in the Mozambique Channel from run 1 for model days 63, 108, 117 and 153. The position of an anticyclonic eddy generated north of Madagascar is marked. Initially, the eddy translates westwards to the coast of Mozambique and then continues northwards and leaves the model domain. All other modeled anticyclones from run 1 that are formed north of Madagascar follow the same route.

Figure 19 shows modeled velocity vectors and sea surface heights in the Mozambique Channel from run 1 for model days 156, 180, 237, 303 and 363. The position of an anticyclonic eddy generated on the west coast of Madagascar, at 16 °S, is marked. The eddy moves south-westward until it reaches 21 °S. Here the anticyclone is trapped and it remains at this location for the rest of the year simulated. None of the anticyclonic eddies generated in run 1 are able to move beyond 21 °S.

Results run 2:

In run 2 modeled anticyclonic eddies in the Mozambique Channel are formed at the northern tip of Madagascar.

Figure 20 demonstrates the migration of an anticyclonic vortex generated north of Madagascar. The figure shows sea surface heights and velocity vectors for model days 91, 163, 208 and 298. Initially the eddy translates westward with an average velocity of 7 $\frac{\text{cm}}{\text{s}}$ (6 $\frac{\text{km}}{\text{day}}$). After reaching the eastern coast of Mozambique it continues southwards through the channel. From 14 °S to 20 °S the eddy has a meridional velocity of 17 $\frac{\text{cm}}{\text{s}}$ (15 $\frac{\text{km}}{\text{day}}$). From 20 °S to 29 °S the eddy's velocity has decreased to 13 $\frac{\text{cm}}{\text{s}}$ (11 $\frac{\text{km}}{\text{day}}$). From the time it is generated, the eddy travels through the Mozambique Channel in approximately 200 days. All other eddies formed north of Madagascar in run 2 follow the same track with similar translation velocities.

Results satellite observations:

Satellite observations show that most anticyclonic eddies in the Mozambique Channel are generated north of Madagascar, but it is also found that anticyclones are formed at the west coast of Madagascar, at approximately 16 °S.

Figure 21 shows observed sea surface heights from satellites in the Mozambique Channel for week 26, 32, 40 and 47 2002. The location of an anticyclonic eddy generated north of Madagascar is marked. The eddy translates westwards with an average velocity of 10 $\frac{\text{cm}}{\text{s}}$ (9 $\frac{\text{km}}{\text{day}}$). It then migrates southwards through the channel along the coast of Mozambique. From 12 °S to 20 °S the eddy has a meridional velocity of 6.5 $\frac{\text{cm}}{\text{s}}$ (5.6 $\frac{\text{km}}{\text{day}}$). From 20 °S to 29 °S the eddy's velocity has increased to 8.7 $\frac{\text{cm}}{\text{s}}$ (7.5 $\frac{\text{km}}{\text{day}}$). The anticyclonic eddy uses nearly 300 days to travel through the channel, from the time it is generated at the northern tip of Madagascar.

In Figure 22, which shows observed sea surface elevation the Mozambique Channel for week 34, 43, 44 ,49 and 52, 2002, the position of an anticyclonic eddy formed at the west coast of Madagascar, is marked. The eddy moves southwestwards towards the coast of Mozambique. Here it merge with a south going anticyclone, generated north of Madagascar. This new eddy then continues southwards through the channel along the coast of Mozambique.

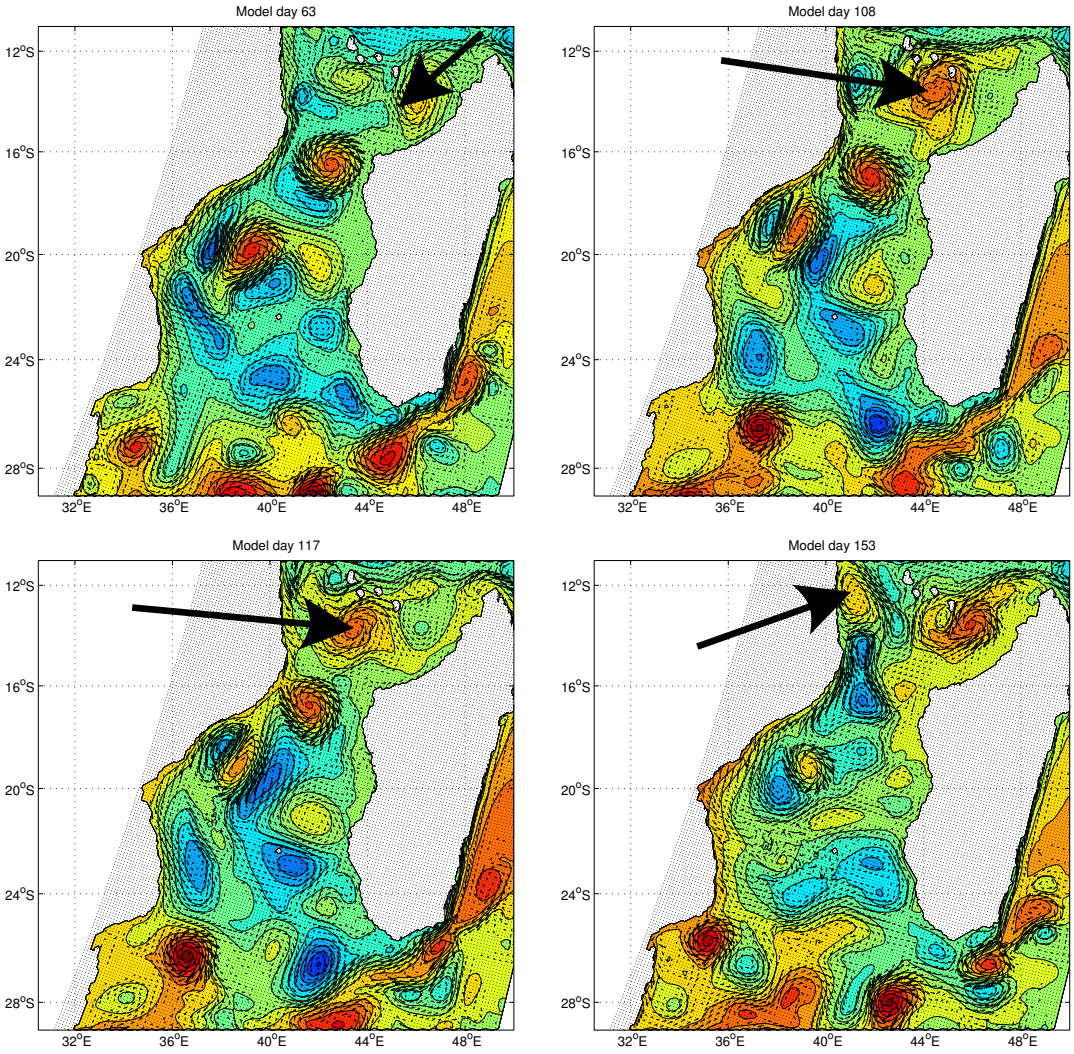

Figure 18: *Results from run 1. Modeled sea surface heights and velocity vectors in the surface layer (σ layer 30) for model days 63, 108, 117 and 153. Note the marked eddy.*

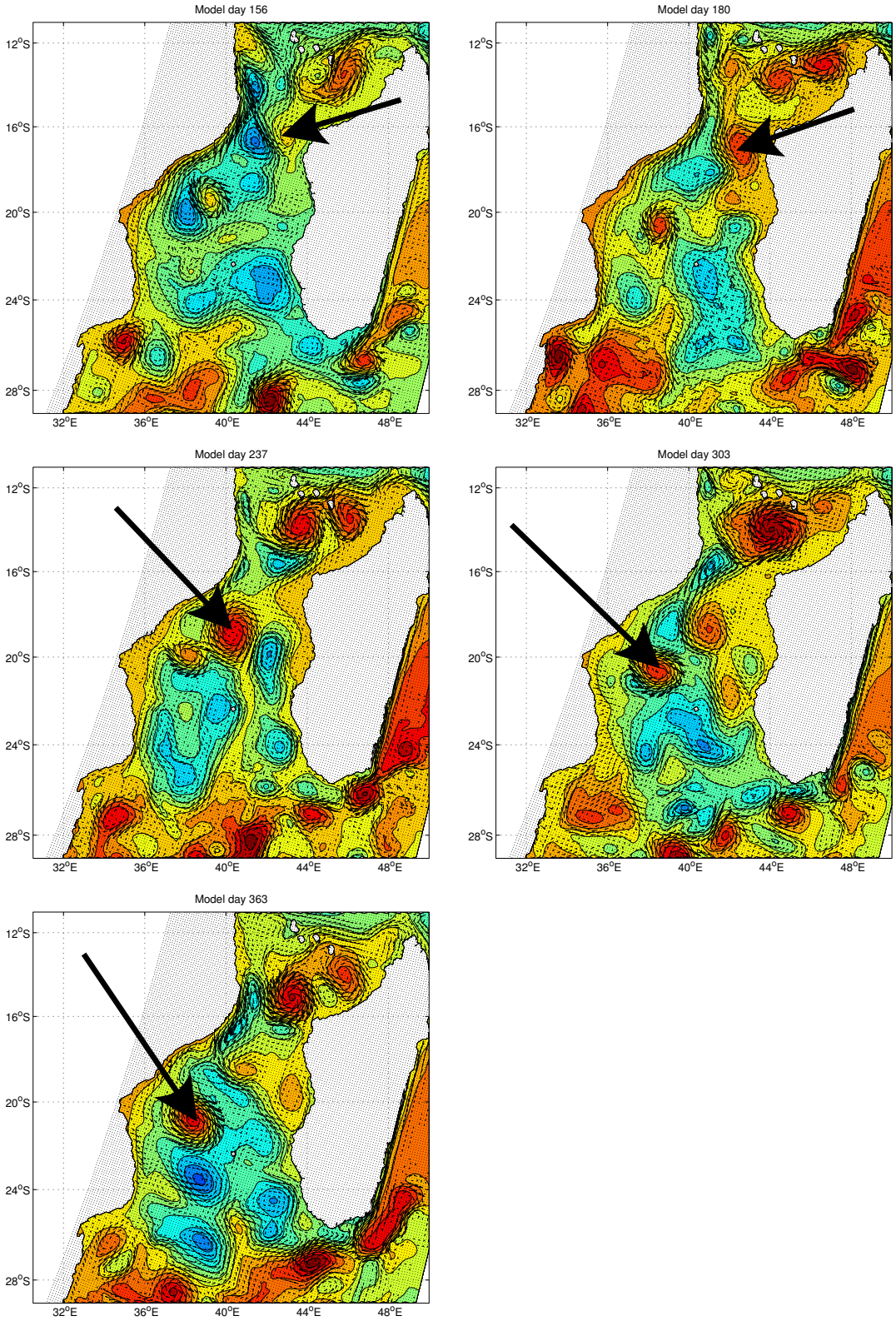

Figure 19: *Results from run 1. Modeled sea surface heights and velocity vectors in the surface layer (σ layer 30) for model days 156, 180, 237, 303 and 363. Note the marked eddy.*

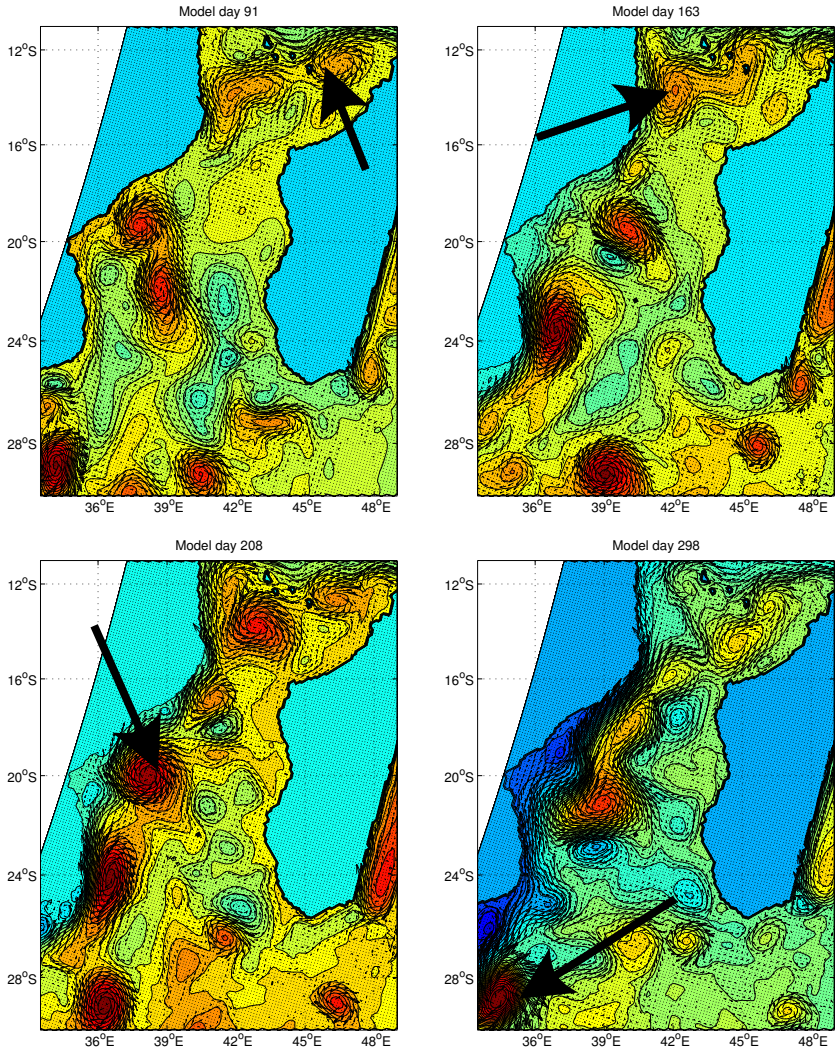

Figure 20: *Results from run 2. Modeled sea surface heights and velocity vectors in the surface layer (σ layer 30) for model days 91, 163, 208 and 298. Note the marked eddy.*

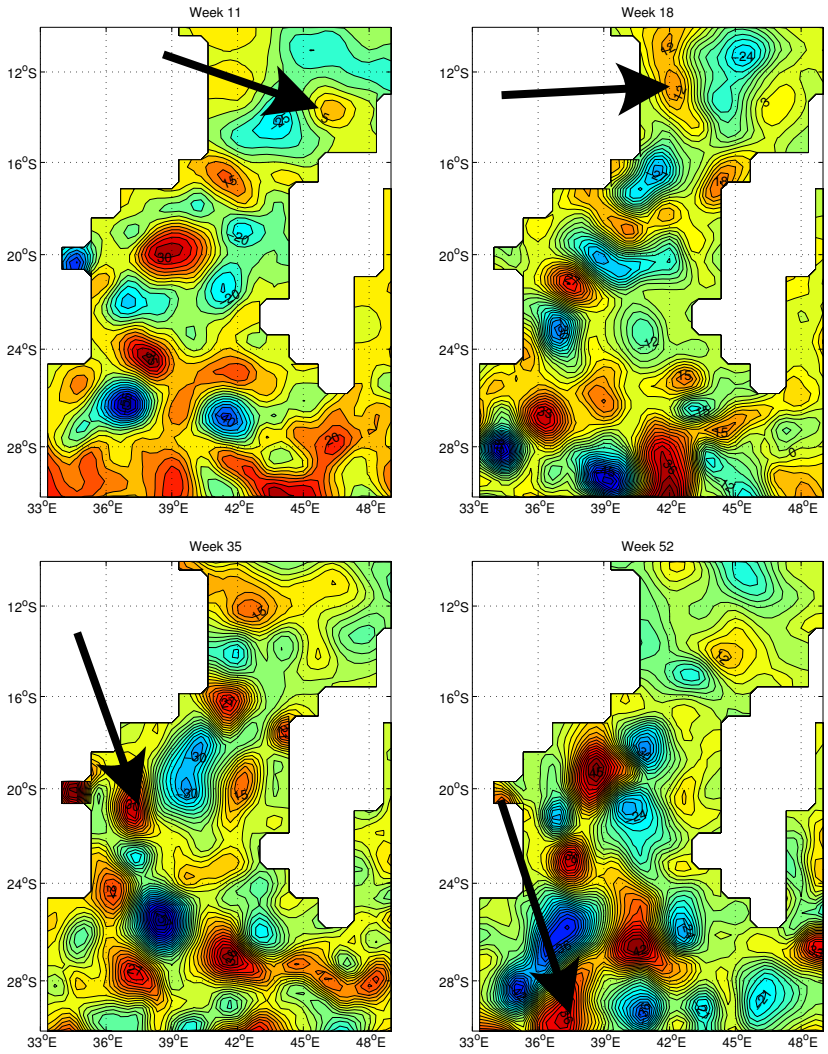

Figure 21: *Results from satellite observations. Sea surface heights for week 11, 18, 35 and 52 the year 2002. Note the marked eddy.*

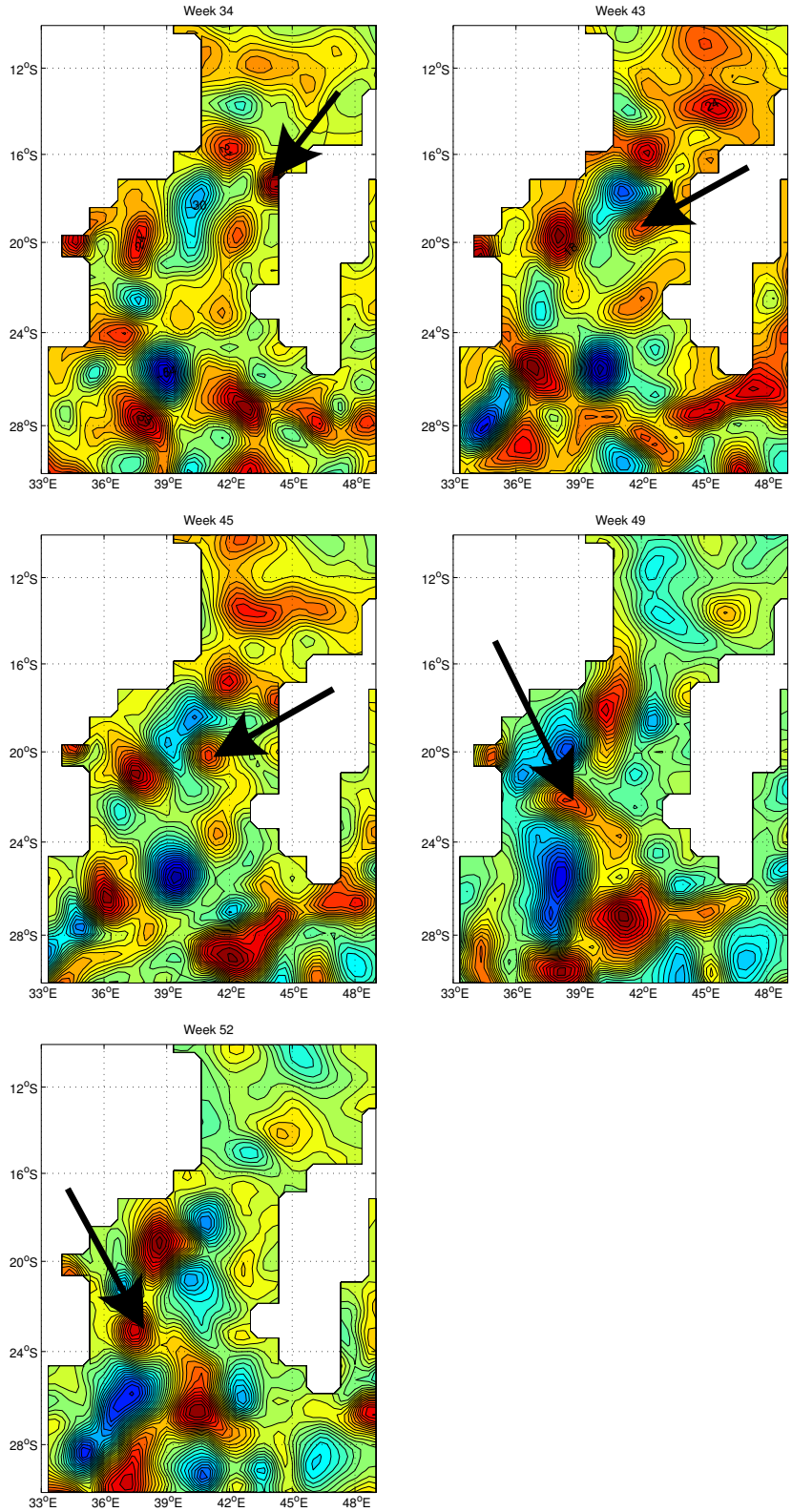

Figure 22: *Results from satellite observations. Sea surface heights for week 34, 43, 45, 49 and 52 the year 2002. Note the marked eddy.*

3.7 Generation mechanism

In this section I will look into the mechanisms responsible for generating modeled anticyclonic vortices north of Madagascar.

To detect the frequency at which modeled eddies are generated, the average sea surface height (SSH) spectra of the generation area is investigated. If one assumes that eddies are stationary in the generation phase, it is possible to find dominant Fourier components of the sea surface heights as a function of time. Observed and modeled SSH spectra near the northern tip of Madagascar are shown in Figure 23. In run 1,

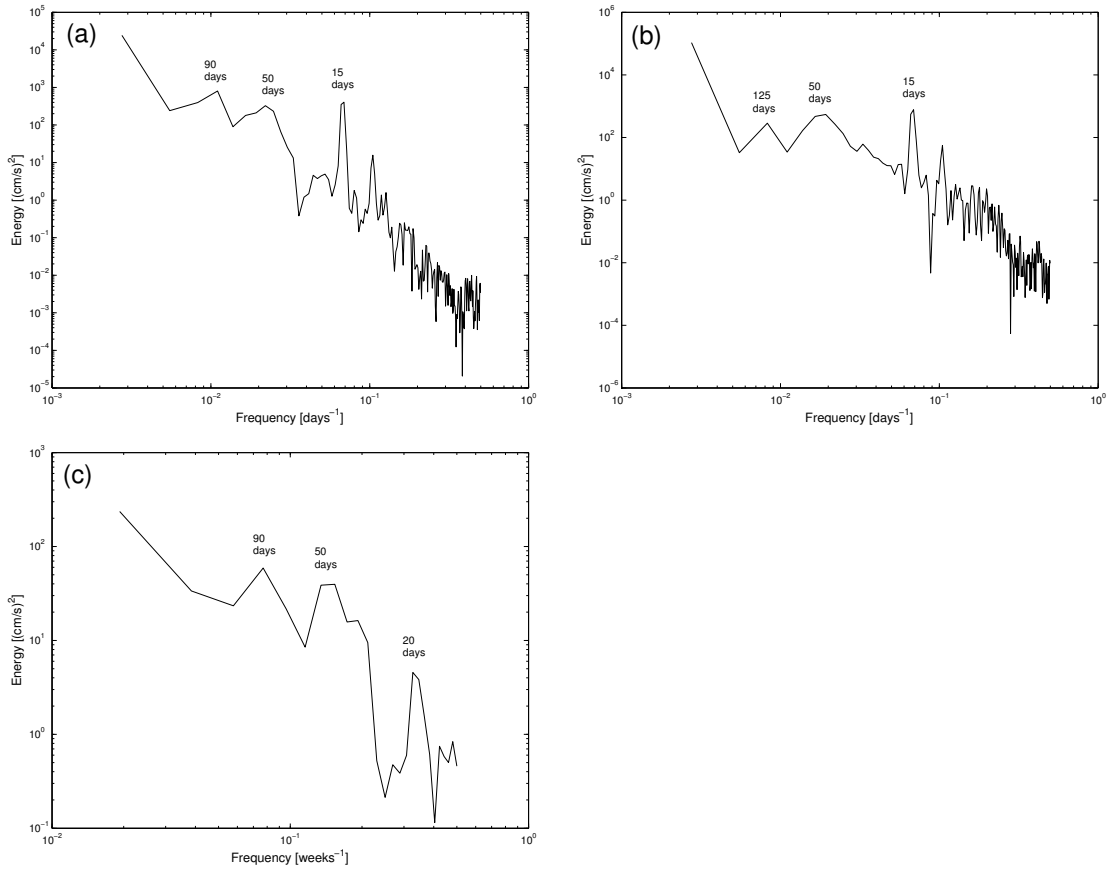

Figure 23: *Modeled and observed SSH spectra near the northern tip of Madagascar. a) shows the result of run 1, b) the result of run 2 and c) satellite results.*

peaks are seen at about 90 days, 50 days and 15 days, where the 90 days period is the most dominant. Run 2 shows peaks at roughly 125 days, 50 days and 15 days, where the 15 days component shows most energy. Satellite results show highest energy for 90 and 50 days, and less energy for the peaks at 20 days.

The mechanisms responsible for the generation of modeled anticyclonic eddies in the

Mozambique Channel can be found by calculating energy interaction terms. The transfer of energy from mean available potential energy to eddy potential energy (T_1) and the transfer of energy from mean kinetic energy to eddy kinetic energy (T_2), are given as (see Appendix A):

$$T_1 = g \cdot \int\int\int \frac{\overline{u' \cdot \rho'} \cdot \frac{\partial \overline{\rho}}{\partial x} + \overline{v' \cdot \rho'} \cdot \frac{\partial \overline{\rho}}{\partial y}}{\frac{d\tilde{\rho}}{dz}} \, \mathrm{d}V$$

$$T_2 = -\int\int\int (\overline{u' \cdot u'} \cdot \frac{\partial \overline{u}}{\partial x} + \overline{u' \cdot v'} \cdot (\frac{\partial \overline{v}}{\partial x} + \frac{\partial \overline{u}}{\partial y}) + \overline{v' \cdot v'} \cdot \frac{\partial \overline{v}}{\partial y}) \, \mathrm{d}V$$

The conversion from mean available potential to eddy potential energy, T_1, can be used as an indicator for baroclinic instability, and the conversion from mean kinetic to eddy kinetic energy, T_2, for barotropic instability (Böning and Büdich, 1992). Baroclinic and barotropic instability describes how fluctuations of the mean flow grow in time. If fluctuations are allowed to grow the flow is unstable (Pedlosky, 1987). The reference state for potential density, the state at which density gradients are strictly vertical, is represented by $\tilde{\rho}$. This is simulated by taking the horizontal average and the time mean of the density field. To achieve good results, global averages and long time periods ought to be used. Here the average has been taken over the model domain and over a time period of one year. The variables u, v and ρ are split into time-mean components and fluctuations; $a = \overline{a} + a'$. The time mean must be chosen in such a way that low frequency variability (for example seasonal variability) is seen as variability of $\overline{a}$, and not included in a'. Dominant periods of the mean flow is found by spectral analysis. Power spectral density distribution of zonal velocity and density for σ layer 28 in run 1, is plotted in Figure 24. Results from run 2 are not shown, but they give similar results. Figure 24 shows velocity and density of the South Equatorial Current

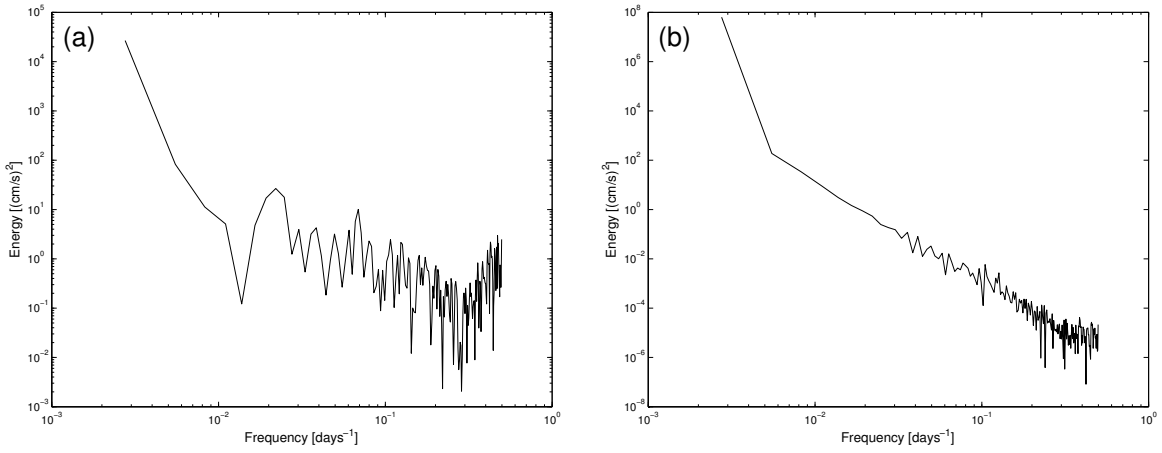

Figure 24: *Power spectral density diagram from run 1. Energy distribution of zonal velocity (a) and density (b) as a function of frequency in the South Equatorial Current.*

at 13.2 °S 51.1 °E. From the figure it is not possible to detect a clear variation period of the mean flow. Therefore even a long averaging period will to a low extend affect the instability terms, T_1 and T_2. The averaging is done over a time period of one year.

T_1 and T_2 are calculated along section CD, which goes from 11.6 °S 47.5 °E to 14.7 °S 42.4 °E (Fig. 25). Figure 26 a), b), c) and d) show the dependency of the two conversion terms T_1 and T_2 per unit mass, along section CD, averaged over the top 500 m layer. Section CD has been chosen since it intersects the generation area north of Madagascar (Fig. 18 and 20).

In run 1, T_1 varies between $-22 \cdot 10^{-4}$ $\frac{\text{cm}^2}{\text{s}^3}$ and $260 \cdot 10^{-4}$ $\frac{\text{cm}^2}{\text{s}^3}$, while T_2 lies in the range $-0.13 \cdot 10^{-4}$ $\frac{\text{cm}^2}{\text{s}^3}$ to $0.14 \cdot 10^{-4}$ $\frac{\text{cm}^2}{\text{s}^3}$
In run 2, T_1 goes from $-111 \cdot 10^{-4}$ $\frac{\text{cm}^2}{\text{s}^3}$ to $182 \cdot 10^{-4}$ $\frac{\text{cm}^2}{\text{s}^3}$ and T_2 from $-0.5 \cdot 10^{-4}$ $\frac{\text{cm}^2}{\text{s}^3}$ to $0.15 \cdot 10^{-4}$ $\frac{\text{cm}^2}{\text{s}^3}$.

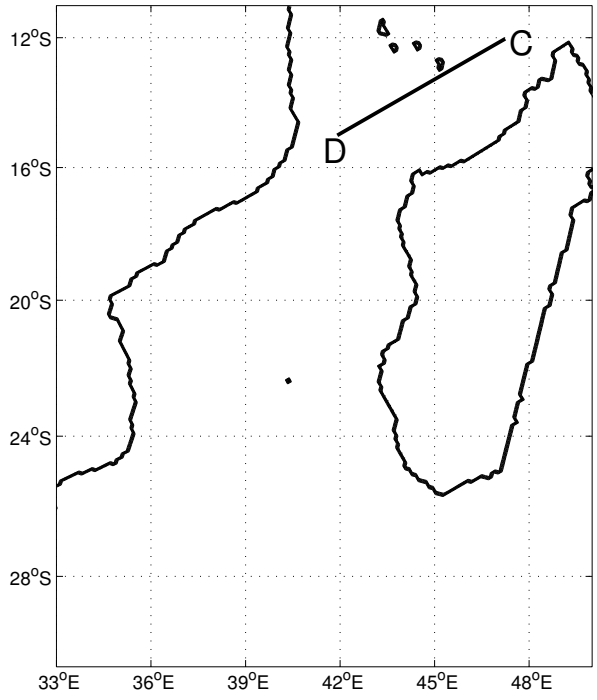

Figure 25: *Section CD: From* 11.6 °S 47.5 °E *to* 14.7 °S 42.4 °E.

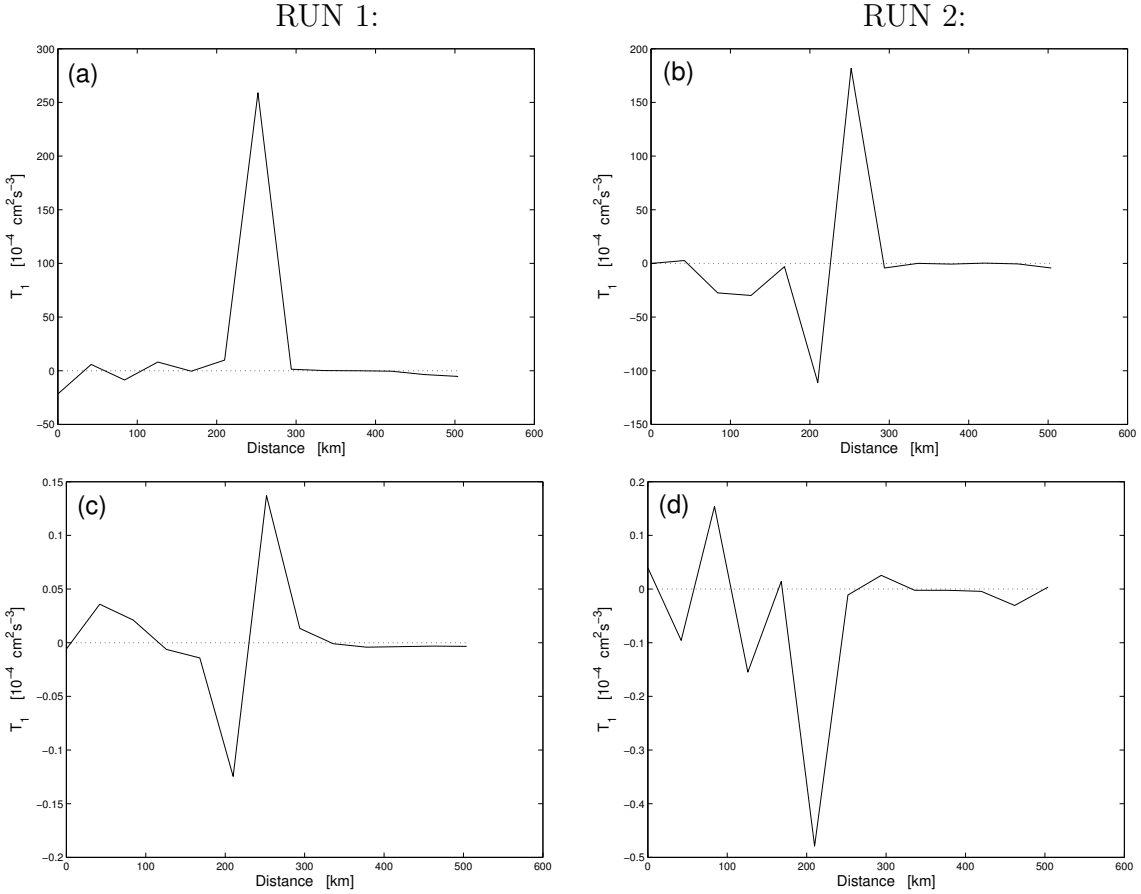

Figure 26: *Term T_1 and T_2 per unit mass averaged over the upper 500 m along section CD: a) T_1 from run 1 b) T_1 from run 2 c) T_2 from run 1 d) T_2 from run 2.*

4 Discussion

4.1 Sea surface temperature

In both run 1 and run 2, the meridional distribution of the sea surface temperature is in agreement with observations (Fig. 3 and 4). The strong decrease in temperature near 22 °S in summer (January) and 24 °S in winter (August) is well reproduced. The surface temperature distribution is mainly dependent on the net solar radiation, heat fluxes between ocean and atmosphere, wind forcing (up/down welling, horizontal advection) and advection of heat through the open boundaries. With these variables fixed to climatology, realistic results are expected. However, in both run 1 and run 2, the temperatures are too low in the western part of the Mozambique Channel in January. In August the sea surface temperatures from run 2 have a distribution similar to observations, but results from run 1 deviates even more from satellite results, with too low temperature values in the western part of the channel.

It is not immediately clear whether the differences seen between model and observations are due to inadequate initial and boundary values, inadequate forcing fields, or errors in the ocean model. However, since the forcing field and inflow is fixed to climatology, the differences are possibly caused by the conditions for outflow at the southern open boundary. It has been shown that the open boundary problem is not well posed for the shallow water equations and the primitive equations (Bennet and Kloeden, 1978), i.e., a set of boundary conditions which guarantees the existence of a stable, unique solution cannot be defined.
I run 1, the boundary values are fixed to climatology. This will generally lead to overspesification, and the solution being approximated will not be continuous. When the propagation is towards the boundary, discontinuities cause reflection of the prognostic variable back into the model domain (Strauss, 1992). Initially (spin up period), the flow is southwards in the western part of the channel and reflections are expected at this side. Since the temperature decreases polewards, colder water is then being advected northwards. In run 1 this is seen as lower values of the sea surface temperature in the western part of the Mozambique Channel.
With adaptive boundary conditions, disturbances are allowed to propagate out of the domain, thus reflections are not expected. Run 2 gives results in agreement with observations in August. In January, temperature values in the western part of the channel are too low, most likely due to the initial conditions, which are obtained from run 1.

4.2 Sea surface height

The high pressures seen in the Mozambique Channel in model results and satellite observations can be attributed to anticyclonic vortices, which are present in the channel.

In eddy motion the balance of forces are usually between the pressure force and the Coriolis force, allthough sometimes also the centrifugal force plays an important role (Cushman-Roisin, 1994). The barotropic contribution of the pressure force is seen as elevation of the sea surface. Figure 27 shows sea surface heights and velocity vectors from run 1 at model day 1. It is seen that areas with increased sea surface height are associated with anticyclonic motion.

Also depressions of the sea surface are seen in the Mozambique Channel, in both observations and model results (e.g. Fig. 5). As seen in Figure 27, only weak cyclonic motion follows modeled depressions. LADCP measurements and drifter data from the Mozambique Channel show no sign of cyclonic vortices, only anticyclones are revealed (Fig. 14, 15 and 16). It can therefore be assumed that depressions of the sea surface are not a result of cyclonic motion, but induced by anticyclonic eddies. Increased sea surface heights at some places must be compensated by lowered sea surface at other places. However, due to the pressure gradient induced by the lowered sea surface, depressions must be accompanied with some cyclonic motion, as the weak cyclonic motion seen in Figure 27.

In Section 3.2 it is found that modeled high pressures from both run 1 and run 2 have a horizontal scale and amplitude of the same order as what is observed, allthough differences are seen. The monthly means of January and August (Fig. 5 and 6) show that anticyclones from run 1 have smaller amplitudes than observations in both January and August, while anticyclones from run 2 have higher amplitudes compared to observations in August. These differences are due to a combination of the generation frequency and the migration of modeled anticyclones, and will be discussed in further details in Section 4.6.

4.3 Transports

Ridderinkhof et al. (2003) found, by use of moored current measurements, the mean volume transport through section AB (Fig. 9) to be -7.2 Sv for 2000/2001. Moored current measurements are, however, sensitive to the location of the instruments. Seen in Figure 10 the eddy's swirl velocity as a function of distance from the eddy's center is not constant. With anticyclonic eddies frequently passing the section, the current measurements might not be able to give a complete description of the volume transport.
DiMarco et al. (2002) gives estimates of volume transports from the last decades in the Mozambique Channel, based on hydrography. Out of eight transport estimates only one give a northward flow in the upper 1500 m depth. That section was located in the eastern part of the channel where the flow is believed to be more northwards (Lutjer-

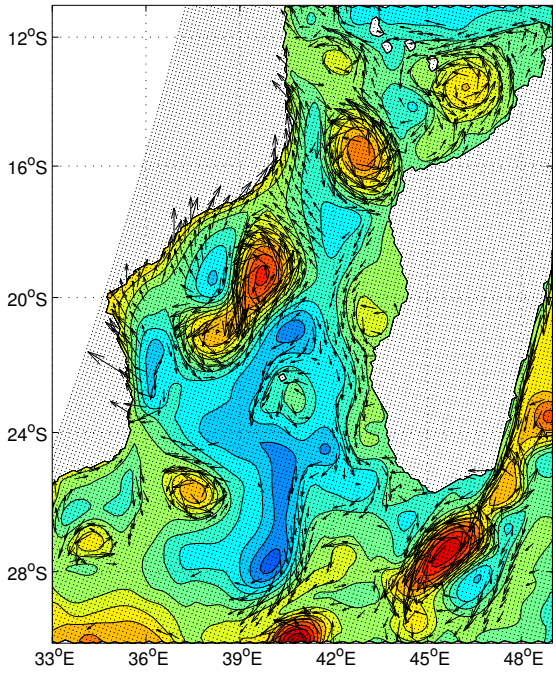

Figure 27: *Modeled sea surface heights and velocity arrows in the Mozambique Channel from run 1 for model day 1. Note that surface elevations (red) are associated with anticyclonic motion*

harms, 2005). The transport results from run 2, which show a southward transport of 3.1 Sv, gives a close estimate of the observed volume transport, while the northward transport found in run 1 (1.7 Sv northward) deviates too much from observations.

The modeled transport estimates show a strong dependency on the conditions at the open boundaries. With the southern open boundary fixed to climatology, reflections occur, which results in a northward mean transport for run 1. Figure 9 a) shows that after a strong northward transport in the first part of the year, the magnitude of the flow decreases, indicating that a steady state is being reached. For run 2, the adaptive boundary conditions allow the flow to propagate out of the domain without reflections. The background flow is discussed in greater details in Section 4.5.2.

4.4 Structure of Mozambique eddies

A striking difference between the model results from run 1 and run 2 is that anticyclonic eddies from run 2 reach much deeper than those from run 1 (Fig. 10 and 11). Eddy 2 reaches down to the bottom ($\sim$ -3000 m) with velocities of 20 $\frac{\text{cm}}{\text{s}}$, while for eddy 1 the velocities are only 5 $\frac{\text{cm}}{\text{s}}$ at 1000 m depth. Also model results that are not presented in this thesis show that eddies from run 1 are shallower than those from

run 2. The horizontal density gradients are similar for eddy 1 and eddy 2. Therefore the high swirl velocities in deeper layers, must be due to a stronger barotropic signal. For eddy 1, maximum surface elevation is less than 25 cm, and the horizontal scale is approximately 200 km (Fig. 10). For eddy 2, the surface elevation is close to 70 cm, and the horizontal scale is roughly 400 km, hence the barotropic pressure gradient of eddy 2 is stronger than that of eddy 1. For eddy 2 the barotropic signal can be seen all the way to the bottom. A consequence of the high modeled velocities in the bottom layer is upwelling of cold water on the slope (Fig. 11). The frictional drag from the ground causes an Ekman transport towards the western shelf and thereby upwelling. With density gradients follow geostrophic velocities, such as the southward flow added to the swirl velocity of eddy 2 (Fig. 13). It is also possible that the depressed sea surface near the coast of Mozambique, seen in model results from run 2 (Fig. 6), is a result of such upwelling.

High surface velocities in the bottom layer agree with observations from LADCP measurements (eddy 3), which show swirl velocities of 10 $\frac{\text{cm}}{\text{s}}$ near the bottom (Fig. 14). However, the vertical velocity gradient ($\frac{\partial u}{\partial z}$, $\frac{\partial v}{\partial z}$) of eddy 3 is weaker than for eddy 1 and eddy 2 (Fig. 10, 11 and 14). Eddy 3 is therefore to a less extend dependent on the barotropic velocity component to transmit this surface signal all the way to the bottom.
Since the LADCP can not measure in the upper 150 m layer, the surface velocity of eddy 3 is estimated from drifter data. The highest swirl velocity found from drifter 2 is 85 $\frac{\text{cm}}{\text{s}}$, at $r = 82$ km (Table 2). The small velocity variations from 82 km to 92 km indicate that 85 $\frac{\text{cm}}{\text{s}}$ is close to the maximum velocity. If it is assumed that the data from drifter 2 can be used to describe the surface velocity of eddy 3, it is seen that this eddy reaches down to the bottom with similar surface velocities as eddy 1. It is then clear that the modeled baroclinic velocity component, and hence the modeled density stratification, is too strong.

4.4.1 Classification of anticyclonic eddies

In geophysical vortex dynamics the dominant forces are usually the pressure force, Coriolis force and the centrifugal force (Cushman-Roisin, 1994). When all three are present, the equation of motion is written like (Gill, 1982):

$$-\frac{u^2}{r} - f \cdot u = -\frac{1}{\rho} \cdot \frac{\partial p}{\partial r}\,, \qquad \text{(gradient} - \text{wind balance)}$$

where r is the distance from the eddy center and $\frac{\partial}{\partial r}$ is the derivative along r, positive away from the eddy center. If the Coriolis force is more dominant than the centrifugal force, the eddy is called quasi-geostrophic. On the other hand, if the two terms are equally important, eddies are called non-linear. The classification is normally carried

out by calculating the Rossby number, $R_0 = \frac{V}{f \cdot L}$ (i.e. the non linear term of gradient wind equation divided on the Coriolis term). Here V is the difference between maximum northward and maximum southward velocity, L is the length scale of these variations and f is the Coriolis parameter.

Modeled Rossby numbers of eddy 1 and eddy 2 are listed in Table 3. V and L are found from Figure 12 and 13. If $R_0 \sim O(1)$ eddies are non-linear, when $R_0 \ll 1$ eddies are termed quasi-geostrophic. Modeled R_0 is of the order equal to 0.1 for both eddies in all depths, with the highest values near the surface. It is then found that the centrifugal force can be neglected and the balance is between the Coriolis force and the pressure force.

In Table 4 the Rossby number of eddy 3 is listed. The Rossby numbers are calculated in the surface layer by use of drifter data (results from Table 2). In deeper layers R_0 is calculated by use of the LADCP results from Figure 14. Again R_0 is of the order equal to 0.1 in all depths. Both modeled and observed anticyclones in the Mozambique Channel will therefore be referred to as quasi-geostrophic.

Depth	Eddy 1	Eddy 2
20 m	0.20	0.27
100 m	0.13	0.25
260 m	0.05	0.18
500 m	0.05	0.15

Table 3: *Modeled Rossby number for eddy 1 and eddy 2*

4.5 Eddy migration

Satellite observations of the surface elevation in the Mozambique Channel for 2002 show that observed anticyclonic eddies generated north of Madagascar travel southwards through the channel, along the coast of Mozambique (Fig. 21). Eddies travel through the channel during a time period of the order equal to one year.
The model simulation run 1, does not reproduce this migration. Anticyclones generated north of Madagascar move northwards instead of southwards after reaching the coast of Mozambique (Fig. 18). Anticyclones formed farther south, on the west coast of Madagascar at approximately 16 °S, are trapped along the coast of Mozambique

Depth	R_0
15 m	0.21
100 m	0.16
260 m	0.12
500 m	0.11

Table 4: *Estimated Rossby number for observed anticyclonic eddies in the Mozambique Channel based on LADCP and drifter data.*

near 21 °S (Fig. 19).
Anticyclonic eddies generated north of Madagascar in run 2 follow a pathway similar to what is observed, as eddies migrate polewards through the channel along the coast of Mozambique, during a time period of the order equal to one year. (Fig. 20).
To explain the movement of modeled and observed anticyclonic eddies in the Mozambique Channel it is necessary to understand the dynamical processes responsible for vortices' movement. The motion of an isolated anticyclonic eddy is determined by a combination of advection by the mean flow and a self induced motion. The self induced motion is described in Appendix B.

4.5.1 Self induced motion

It is observed that anticyclonic eddies generated north of Madagascar translates westward (Fig. 18, 20 and 21). This zonal drift is called the β drift (Nof, 1981). β is the meridional gradient of the Coriolis parameter. The β drift results from a balance between the northward β force, which is caused by the symmetry of the eddy and the fact that the Coriolis increases away from the equator, and the southward directed Coriolis force, which is acting on the eddy as a solid body (Appendix B). Near a western boundary (coast of Mozambique) the β induced westward drift ceases. After Shi and Nof (1994) an anticyclonic eddy along a vertical wall is affected by the northward directed β force, which is no longer balanced by Coriolis, and two poleward directed forces which results from the eddy-wall interaction: The mirror image of the eddy on the boundary (image effect), and the rocket effect, generated by the loss of anticyclonic fluid (Appendix B). For a sloping boundary (shelf) eddies are also being pushed northwards by the topographical β effect (Matsuura and Kamachi, 1993).

It is still unclear which of these dynamical effects that will have greatest influence on the eddy's meridional movement. An analysis carried out by Shi and Nof (1994)

indicates that all three are of the same order of magnitude. However, their conclusion is that the image effect will be dominant for both quasi-geostrophic and non-linear eddies as the eddy will adjust to the wall by transforming into a half circular vortex along the wall, and thereby increasing the effect by the mirror image. Zavala et al. (1998) introduced a modification of this statement by suggesting that the image effect is only important for quasi-geostrophic eddies as they are the only ones that can adjust to the wall. They also concluded that the rocket effect is only important for short time periods, indicating that the push from the β induced westward drift is temporal.

Modeled and observed anticyclones in the Mozambique Channel have a Rossby number of the order equal to 0.1 in the upper 500 m layer and will be considered to be quasi-geostrophic. With the assumption of the coast as a vertical wall this shall according to the theory mean that the mirror effect is dominant, and give a self induced migration directed polewards. On the other hand, with a sloping coast, eddies are not allowed to adjust to the boundary the same way as they will when the wall is vertical. A sloping boundary will also introduce the effect of the topographical β. It is therefore very difficult to predict the direction of the self induced motion. It is, however, possible to discuss if the model reproduces the self induced motion in a realistic way. The existing theory mainly separates between quasi-geostrophic eddies and non-linear eddies (Shi and Nof, 1994; Zavala et al., 1998). For both runs modeled anticyclones are found to be quasi-geostrophic, the same as observed eddies, which indicates that the self induce motion is similar for modeled and observed anticyclonic eddies in the Mozambique Channel.

4.5.2 Advection by the background flow

In addition to the self induced motion, advection by the background flow influences the meridional migration of anticyclonic eddies in the Mozambique Channel. The importance of the background flow is illustrated by the following example: The background flow needed to compensate for the β induced northward migration, and keep an anticyclonic eddy in a fixed position, can be calculated as in Bowman (1985). For the anticyclonic vortices in the Mozambique Channel, the velocity at 21 °S is found to be less than 5 $\frac{\text{cm}}{\text{s}}$ southwards (Appendix C). This corresponds to a volume transport in the upper 500 m through section AB (Fig. 7), of -6.25 Sv. It is seen that for run 2 the transport through AB is often higher than 6.25 Sv southwards allthough the mean value is less. Therefore, the advection by the background flow will in general be more important than the self induced motion. To properly model the circulation in the Mozambique Channel, further focus must therefore be placed on the background flow.

In austral summer the mean wind direction in the Mozambique Channel is uniformly

from a south-easterly direction (Lutjerharms, 2005). From Gill (1982) is found that on the southern hemisphere, the Ekman transport is 90 ° to the left of the wind direction, which gives an Ekman transport towards south-west in the Mozambique Channel in austral summer.
In the winter the southern part of the channel still experiences south-easterly winds, while in the northern part winds are north-westerlies. This wind regime induces Sverdrup transports, that can be calculated as follows (Gill, 1982):

$$v = \frac{1}{\rho \cdot \beta \cdot H} \cdot \vec{k} \cdot \nabla \times \vec{\tau}_s \ , \tag{7}$$

where H is the equivalent forcing depth, β is the meridional gradient of the Coriolis parameter and τ_s is the surface wind stress. From Equation (7) it is seen that v is negative, and the Sverdrup transport is polewards through the open channel.
Still, allthough the wind forcing shows that the flow is southwards through the Mozambique Channel, it is demonstrated in the model results from run 1, that realistic wind forcing alone is not enough to ensure a poleward background flow. As has been shown, when the boundary values are fixed to climatology, reflections occur at the southern open boundary, and hence the background flow becomes northwards.

4.5.3 Trapping of anticyclonic eddies in the Mozambique Channel

Even without a mean southward background flow, anticyclones in run 1, formed at the west coast of Madagascar at approximately 16 °S, are able to move as far south as 21 °S. This can be explained either by variability in the background flow, so that the eddies are advected southwards when the flow is in that direction, or by the self induced motion, as described previously. West of eddy 1, which is formed at the west coast of Madagascar at 16 °S, a northward flow is observed (Fig. 12). This flow can be interpreted as a leakage of the anticyclone, i.e. the rocket effect, which forces the eddy polewards. However, none of the modeled eddies in run 1 are able to move beyond 21 °S. Not only modeled eddies are trapped at this latitude. From the drifter data it is seen that also observed anticyclones are stationary in this area. Drifter 2 is trapped for more than five months (Fig. 16). It has been controlled by use of satellite observations from 2000 that during this period the sea surface is increased in this area, confirming the presence of an anticyclonic vortex.

The reason for anticyclonic eddies sensitivity to the area near Mozambique at 21 °S is possibly found in the bottom topography. In Figure 10 and 11, one can see a bump in the ocean floor, at roughly 300 km from the slope. If velocities are nonzero in the bottom layer, variations in bathymetry will affect the pressure/Coriolis induced motion (swirl velocity) in all layers, since the near geostrophic swirl velocity can communicate between density layers through the Margules relationship (e.g. Svendsen et al., 1991).

Changes in swirl velocity can again affect the rocket effect. In the barotropic case, a bump in the ocean floor is known as the Taylor column (Kundu, 2005). Under barotropic conditions the vertical gradient of horizontal velocity is zero, and the flow is either stopped or forced around the bump. For a stratified ocean, an adjustment of the pycnocline can be sufficient to allow the flow to pass the bump.

Observed anticyclonic eddies in the Mozambique Channel reach deep and are less stratified than modeled eddies. It is therefore possible that these can be stopped at 21 °S due to the bathymetry. Anticyclonic eddies in run 2 are more stratified, but also they reach deep. In Figure 11 it is seen that eddy 2 passes the bump on the western side of it, as if it is forced around it.

Anticyclones from run 1 are shallower, it is in Figure 10 seen that the swirl velocity of eddy 1 vanishes at approximately 1000 m depth. Still, the eddy is stopped near the bump, and not able to pass through it.

4.6 Generation mechanism

Differences in the SSH spectra in the generation area north of Madagascar, between model results and observations, are demonstrated in Figure 23. The 90 days period is present in run 1 and satellite observations, but not in run 2. The 50 days periodicity is, however, seen in all results. Further, in model results peaks are demonstrated at 15 days, for run 2 it is the dominant period, while it is also significant in run 1. In observations, less energy is concentrated at high frequencies. Still, small peaks in the SSH spectra at 20 days are observed (Fig. 23). In run 2 a periodicity of 125 days is also seen. It is unclear if, and in that case how, anticyclones are generated at these periods. As an introduction to the subject I will present some previous work done on the generation of anticyclonic eddies north of Madagascar.

In 6 years of combined TOPEX/Poseidon and ERS1/2 altimeter data, eddies in the Mozambique Channel have been tracked by manually following the positive SSH anomalies through the Mozambique Channel (Schouten et al., 2003). Between 1995 and 2000, on average 4 eddies per year are found to propagate through the channel. This is in agreement with the 90 days period seen in the SSH spectra (Fig. 23). Further, according to Schouten et al. (2002), the 90 days period is a result of westward propagating Rossby waves. Their interaction with Madagascar pinches of anticyclonic eddies at a 4 per year frequency. How this process takes place is unclear.
With a peak in the SSH spectra at 50 days it is expected that anticyclonic eddies propagate through the channel at a frequency of 7 eddies per year. This has not been demonstrated in satellite observations, but current measurements at 17 °S show sign of a weaker 7 per year frequency in addition to the dominant 4 eddies per year frequency (Ridderinkhof and De Ruijter, 2003). The presence of anticyclonic eddies formed at periods other than the 90 days period, can also be verified by a study of the sea level heights associated with anticyclones in the Mozambique Channel. It is found that the increase in observed SSH anomalies, as the eddies propagate polewards through the channel, can not be explained by conservation of potential vorticity alone (Schouten et al., 2003). It is therefore likely that merging with eddies generated at different frequencies occur, such as the 7 per year frequency. In the model setup of Biastoch and Krauss (1999) modeled anticyclones north of Madagascar are formed at a 7 per year frequency (55 days period) where all eddies propagate through the Mozambique Channel as independent features. Biastoch and Krauss found these anticyclonic vortices to be generated by barotropic instability of the South Equatorial Current (SEC). Barotropic instability of SEC has been demonstrated at a 50 days period also in previous work (e.g. Quadfasel and Swallow, 1986; Schott et al., 1988). Allthough they are overestimated in the model setup of Biastoch and Krauss, it seems possible that anticyclonic vortices north of Madagascar are formed by barotropic instability at a 50

- 55 days period.

4.6.1 Baroclinic instability of the South Equatorial Current

The modeled interaction terms, T_1 and T_2, calculated along section CD (Fig. 25) indicate that in both run 1 and run 2, instabilities of SEC grow on the available potential energy, rather than the work of the Reynolds stresses on the mean shear (Fig. 26). Therefore existing theory that describes the baroclinic instability process will be applied to see if conditions are favorable for instabilities to grow by drawing potential energy from the mean state. The theory is from Cushman-Roisin (1994) and Wright (1987). It considers a geostrophic flow with a vertical shear.

From the quasi-geostrophic equations, potential vorticity $\overline{q}$, is given as (Cushman-Roisin, 1994):

$$\overline{q} = \frac{\partial^2 \overline{\Psi}}{\partial y^2} + \frac{f_0^2}{N^2} \cdot \frac{\partial^2 \overline{\Psi}}{\partial z^2} + \beta_0 \cdot y \ , \tag{8}$$

The stream function of the basic flow is given by Ψ ($-\frac{\partial \Psi}{\partial y} = \overline{u}$), N is the stratification frequency ($N^2 = -\frac{g}{\rho_0} \cdot \frac{d\overline{\rho}}{dz}$) and f_0 is the Coriolis parameter.

Necessary conditions for baroclinic instability to occur are that over a two dimensional vertical section in north-south direction, either (Cushman-Roisin, 1994):

(1) $\frac{\partial \overline{q}}{\partial y}$ changes sign in the domain, or
(2) the sign of $\frac{\partial \overline{q}}{\partial y}$ is opposite to that of $\frac{\partial \overline{u}}{\partial z}$ at the top, or
(3) the sign of $\frac{\partial \overline{q}}{\partial y}$ is the same as that of $\frac{\partial \overline{u}}{\partial z}$ at the bottom.

An easy way to investigate if criteria 1 is fulfilled is found in Wrigth (1987). $\frac{\partial \overline{q}}{\partial y}$ can be rewritten like (Appendix D) :

$$\frac{\partial \overline{q}}{\partial y} = \beta - \frac{\partial^2 \overline{u}}{\partial y^2} - f \cdot \frac{\Delta z}{\Delta y}|_{\rho = constant} \ , \tag{9}$$

Under the assumption that β and north-south variations of $\overline{u}$ are negligible, this result implies that for instabilities to exist, the slope of density contours must be positive for some depths while negative for others. Figure 28 a) and b) show sections of modeled density from run 1 and run 2. The sections go from 13.5 °S 51 °E to 12.9 °S 51 °E, which is within SEC. Both figures show that near the surface the density gradients are negative, while deeper the gradients have changed sign and become positive. It follows that under the assumptions made, the necessary condition for instability given by (1) is satisfied. However, the conclusions are vague and can only say that baroclinic instability is possible in the Mozambique Channel. If the mean flow $\overline{u}$ is known by an

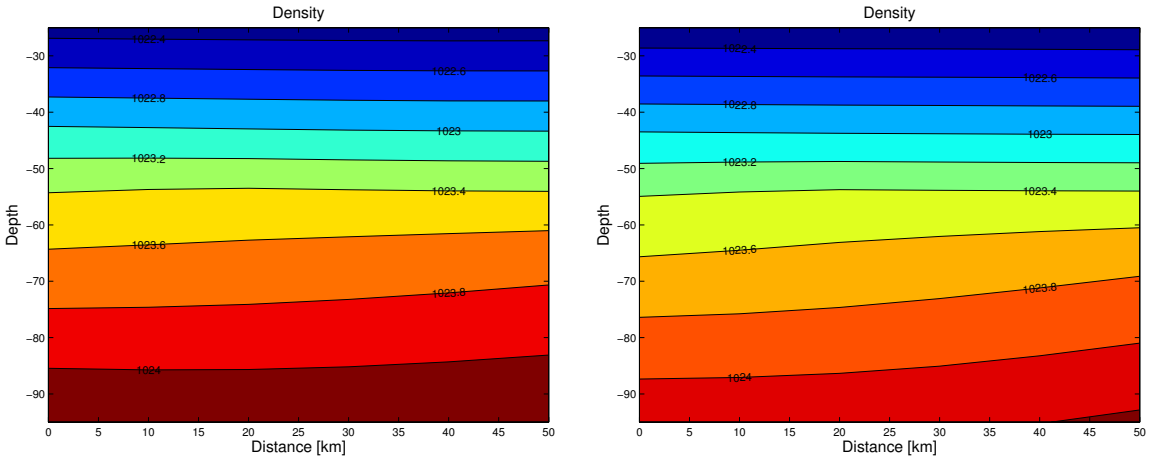

Figure 28: *Section of modeled density from a): run 1 and b): run 2 for model day 64. The section goes from* 13.5 °S 51 °E *to* 12.9 °S 51 °E

expression, more can be said about the instability processes. Figure 29 shows modeled vertical velocity profile of SEC at 13.0 °S 51 °E, for run 1 and run 2. In the upper

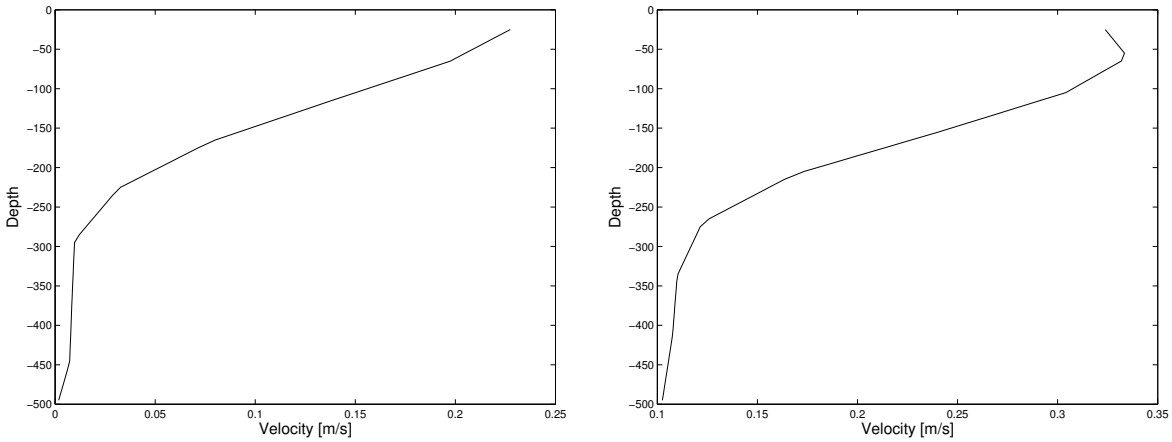

Figure 29: *Vertical profile of the mean flow a): run 1 and b): run 2 at* 13.0 °S 51 °E *for model day 64.*

250 m depth both profiles show a strong vertical velocity gradient, with a linear depth dependency. From 250 m down to 500 m depth velocities are near constant. In the upper 250 m depth velocities can be written like $\overline{u} = U_0 + \alpha \cdot z$, where α and U_0 are constants. If it again is assumed that variations in north-south direction can be neglected, it follows from Cushman-Roisin (1994), that disturbances with wavelength longer than $2.6 \cdot R$ can grow on the available potential energy and is unstable. The Rossby radius is expressed as $R = \frac{N \cdot H}{f}$. The fastest growing disturbances have a wavelength of $3.9 \cdot R$. Disturbances with wavelengths longer than $2.6 \cdot R$ will always occur sooner or later in a persistent flow (Cushin-Roisin, 1994). Under the simplifications

made, baroclinic instability is therefore a plausible generation mechanism for modeled anticyclonic vortices north of Madagascar.

Allthough it is likely that baroclinic instability of SEC plays a role in generating modeled anticyclones in the Mozambique Channel, it is unknown at which period these eddies are generated. The process is not expected to prefer any specific frequency as it is not a cyclic occurrence. It is, however, seen from Figure 23 that in both model runs a significant amount of energy is concentrated at the 15 days period, which can not be explained by either westward traveling Rossby waves or barotropic instability of SEC. It can then be assumed that in the model, anticyclonic eddies are generated by baroclinic instability at a 15 days period. Satellite observations of SSH spectra (Fig. 23) show little energy at this period, indicating that baroclinic instability is a computational phenomenon in the Mozambique Channel. It is seen in the velocity structure of eddy 1, eddy 2 and eddy 3 (Fig. 10, 11 and 14) that modeled vertical gradient of swirl velocity is stronger than what is observed from LADCP measurements, indicating a steeper density gradient in the model. Strong stratification is in favor of baroclinic instability. Too strong density stratification therefore leads to an overestimation of modeled anticyclonic eddies, in both run 1 and run 2.
The rapid formation of anticyclones, again causes an overestimation of modeled sea surface heights in run 2, as seen in Figure 6 c). When eddies are generated at such a short period as 15 days these will merge with eddies generated at the same frequency, as well as other eddies. In run 1, however, the generation of modeled anticyclones at the 15 days period will not affect the circulation in the channel, as these eddies are advected northwards and out of the model domain.

4.6.2 Westward traveling Rossby waves

The last aspect of the generation mechanism is the formation of anticyclonic eddies induced by westward traveling Rossby waves at the 90 days period. It seems likely that it is the landmasses of Madagascar that make this generation possible. A detailed description of this type of eddy formation is complex, and missing in literature. Some general aspects are discussed in Pedlosky and Spall (1999). Allthough it is beyond the scope of this thesis to investigate how Rossby waves can induce the generation of anticyclonic vortices north of Madagascar, it is natural to look into how this process can be reproduced in the model.
Figure 23 shows that peaks in the SSH spectra at 90 days are only seen in run 1 and in satellite observations. For run 2 a weaker signal is seen at 125 days. If the 90 days signal that is seen in the SSH spectra in run 1 is due to Rossby waves, it must be attributed to the conditions at the open boundary in the north-eastern corner of the model domain. From Lutjerharms (2005) the regions north-east of Madagascar are subject to inflow

of SEC, i.e. the boundary is active and force the interior solution. Then climatology is sufficient as boundary condition. With a high enough spatial resolution, the Rossby wave signal can communicate through the boarder and contribute to the formation of anticyclonic eddies in the Mozambique Channel at a period of 90 days. In run 2 different boundary conditions are used. Under inflow conditions they are equal to the climatology conditions, but they also allow outward propagation when the phase speed normal to the boundary is positive. Due to the fact that perfect boundary conditions do not exist (Bennet and Kloeden, 1978), outward propagation may occur at times where propagation should be inwards. For example, the phase speed is calculated directly from the radiation equation (Equation 3) which assumes the Φ field to be slowly varying in time. This can not be guarantied if the forcing field is strong. Further, it has been assumed that the zonal variations of SEC are small, but these are important when calculating the phase speed, and thereby determining whether radiation conditions or external values should be applied at the open boundary. With $\frac{\partial u}{\partial x} \sim 0$ a horizontal resolution of 10 km may not be sufficient to determine the sign of $\frac{\partial u}{\partial x}$. It is then seen that the adaptive boundary conditions are not necessarily capable of determining if the flow is inwards or outwards. Of that reason, the Rossby wave induced anticyclones, generated at a four per year frequency, may not be reproduced in run 2.

5 Summary

In the model simulation of the circulation in the Mozambique Channel, some general aspects have been made clear. First of all this regards the great importance of the conditions at the open boundaries. The model has been run with boundary conditions fixed to climatology (run 1) and with adaptive boundary conditions (run 2), that allows disturbances to propagate out of the model domain.

In both runs anticyclonic eddies are formed at the northern tip of Madagascar. In run 2 these are advected southwards by the background flow along the coast of Mozambique. In run 1 the background flow in the channel is directed northwards due to reflections at the southern open boundary, with the result that anticyclonic eddies formed north of Madagascar are advected towards the equator. In run 1 anticyclonic vortices are also generated at the western coast of Madagascar, near 16 °S. During the year simulated two eddies are formed at this location. Both migrate polewards, but are stopped at 21 °S near the coast of Madagascar, possibly due to horizontal gradients of the bottom topography.

It is found that in both model runs anticyclonic eddies north of Madagascar are generated by baroclinic instability at a 15 days period. This is in contrast to satellite observations, which only show weak sign of eddies generated at this high frequency. A possible reason for the differences seen, are too strong stratification in the model, which is in favor of baroclinic instability.
Satellite observations and previous work (Schouten et al., 2003) indicate that anticyclones north of Madagascar are generated by barotropic instability at a 50 - 55 days period, and by westward traveling Rossby waves at a 90 days period. Peaks in the Sea Surface Height spectra at the 50 days period are seen in both model runs, while the 90 days period is only seen in run 1. The reason for the 90 days period to be missing in run 2 can possibly be due to the conditions at the north-eastern open boundary. With values fixed to climatology the Rossby wave signal is transmitted into the model domain, while when adaptive conditions are used the signal may not transmitted.

It is indicated from the vertical gradient of swirl velocity that the modeled density field has too strong stratification compared to observations. Still, in run 2 the barotropic swirl velocity signal of anticyclonic eddies are seen all the way down to the bottom ($\sim$ -3000 m). The great surface elevation can be attributed to the high frequency of which modeled anticyclones north of Madagascar are generated at. When eddies are generated at such a short period as 15 days, a possibility exists that these may merge with eddies generated at the same frequency as well as other eddies. In run 2, where the anticyclonic eddies formed north of Madagascar migrate southwards through the

channel, such merging quit clearly takes place. In run 1 eddies travel north and out of the model domain and merging of these do not occur.
The anticyclonic eddy from run 1, that is hydrographically investigated at 21 °S (Fig. 10), is formed at the west coast of Madagascar near 16 °S. During the year simulated only two eddies are formed at this location. It is seen that this eddy only reaches down to roughly 1000 m depth. The barotropic signal is strongly dependent on the generation frequency and eddies ability to interact with each other. Therefore, anticyclones from run 1 have lower surface elevation and are shallower than those seen in run 2.

Future work

To gain better understanding of the circulation in the Mozambique Channel by use of numerical models the validation of these models must be extensive and accurate. As future model setups should seek for a more detailed description of the circulation in the Mozambique Channel, more observations must be done.
Further, better reproduction of density stratification is needed to avoid generation of anticyclonic eddies at a too high frequency as a result of baroclinic instability. Also, higher resolution of the model domain will give a more detailed description of the circulation. Especially, for information that is determined outside the model domain to force the interior solution (inflow of the South Equatorial Current), high resolution is needed and values at the boundary must ensure inflow at all times. In those cases boundary values fixed to climatology is preferred. At the southern open boundary adaptive boundary conditions must be used, so that the interior solution is allowed to propagate out of the domain without being reflected.

A Baroclinic and barotropic instability terms

A detailed derivation of the two energy conversion terms, T_1 and T_2, is difficult to find (or missing) in the literature. Therefore this appendix has been made as a suggestion of how to outline these conversion terms.

Available potential energy

Available potential energy in a volume V is given as (Oort et al, 1989):

$$P = \int\int\int \rho \cdot g \cdot z \, \mathrm{d}x \, \mathrm{d}y \, \mathrm{d}z - \int\int\int \rho \cdot g \cdot z_r \, \mathrm{d}x \, \mathrm{d}y \, \mathrm{d}z \ , \tag{10}$$

where z_r is the reference level of which the horizontal density gradients are zero and the equations are integrated over V.

Changing from the (x, y, z) to (x, y, ρ) coordinates, and integrate by parts, one gets:

$$P = A + B \ , \tag{11}$$

$$A = \int\int \rho \cdot g \cdot \frac{z^2}{2} \, \mathrm{d}x \, \mathrm{d}y + \int\int \rho \cdot g \cdot \frac{z_r^2}{2} \, \mathrm{d}x \, \mathrm{d}y \ , \tag{12}$$

$$B = \int\int\int g \cdot \frac{z^2}{2} \, \mathrm{d}x \, \mathrm{d}y \, \mathrm{d}\rho - \int\int\int g \cdot \frac{z_r^2}{2} \, \mathrm{d}x \, \mathrm{d}y \, \mathrm{d}\rho \ , \tag{13}$$

Here A is evaluated at $\rho = \rho_1$ and ρ_2, corresponding to z at the surface and the deepest level. Both layers are usually close to horizontal so that $A \approx 0$.

B can be written:

$$B = g \cdot \int\int\int (\frac{z^2}{2} - \frac{z_r^2}{2}) \, \mathrm{d}x \, \mathrm{d}y \, \mathrm{d}\rho = \frac{g}{2} \cdot \int\int\int (z - z_r)^2 \, \mathrm{d}x \, \mathrm{d}y \, \mathrm{d}\rho \quad + \\ \frac{g}{2} \cdot \int\int\int (2 \cdot z_r \cdot z - 2 \cdot z_r^2) \, \mathrm{d}x \, \mathrm{d}y \, \mathrm{d}\rho \ , \tag{14}$$

Since the density surfaces in the reference state are horizontal one can write:

$$\int\int\int z_r \cdot (z - z_r) \, \mathrm{d}x \, \mathrm{d}y \, \mathrm{d}\rho = \int z_r \cdot (\int\int (z - z_r) \, \mathrm{d}x \, \mathrm{d}y) \, \mathrm{d}\rho \ ,$$

Consider a large horizontal area so that:

$$\int\int (z - z_r) \, \mathrm{d}x \, \mathrm{d}y \approx 0 \ , \tag{15}$$

It then follows that Equation (13) can be written as:

$$\frac{g}{2} \cdot \int\int\int (z - z_r)^2 \, \mathrm{d}x \, \mathrm{d}y \, \mathrm{d}\rho \, , \tag{16}$$

z_r is then replaced with the global mean height over a constant density surface $\tilde{z}$=$\tilde{z}(\rho)$. It is assumed that the horizontal density gradients are negligible. Going from ρ coordinates to z coordinates, P is found to be :

$$P = -\frac{g}{2} \cdot \int\int\int (z - \tilde{z})^2 \cdot \frac{\partial \tilde{\rho}}{\mathrm{d}z} \, \mathrm{d}x \, \mathrm{d}y \, \mathrm{d}z \, , \tag{17}$$

For small perturbations $z - \tilde{z} \ll 1$, $\rho(z)$ is given as:

$$\rho(z) \approx \rho(\tilde{z}) + \frac{\partial}{\partial z}\rho(\tilde{z}) \cdot (z - \tilde{z}) \, ,$$

which gives :

$$z - \tilde{z} = \frac{\rho - \tilde{\rho}}{\frac{\partial \tilde{\rho}}{\partial z}} \, ,$$

and P can be written as:

$$P = -\frac{g}{2} \cdot \int\int\int \frac{(\rho - \tilde{\rho})^2}{\frac{\partial \tilde{\rho}}{\partial z}} \, \mathrm{d}y \, \mathrm{d}x \, \mathrm{d}z \, , \tag{18}$$

Mean and eddy available potential energy

Divide ρ into a time-mean component and fluctuations (ρ =$\overline{\rho}$ + ρ') so that

$$\frac{\overline{(\rho - \tilde{\rho})^2}}{\frac{\partial \tilde{\rho}}{\partial z}} \, ,$$

can be written like:

$$< \frac{\overline{\rho}^2 + \rho'^2 + \tilde{\rho}^2 - 2 \cdot (\overline{\rho} + \rho') \cdot \tilde{\rho} - 2 \cdot \rho' \cdot \tilde{\rho}}{\frac{\partial \tilde{\rho}}{\partial z}} > \, ,$$

$<$ $>$ denotes a time mean. The time mean of fluctuations is 0.

The time mean of the available potential energy can be divided into mean potential energy (PEM) and eddy available potential energy (EPE) given as:

$$EPE = -\frac{g}{2} \cdot \int\int\int \frac{\overline{\rho'}^2}{\frac{\partial \tilde{\rho}}{\partial z}} \, \mathrm{d}y \, \mathrm{d}x \, \mathrm{d}z \, , \tag{19}$$

$$PEM = -\frac{g}{2} \cdot \int\int\int \frac{(\overline{\rho} - \tilde{\rho})^2}{\frac{\partial \tilde{\rho}}{\partial z}} \, \mathrm{d}y \, \mathrm{d}x \, \mathrm{d}z \, , \tag{20}$$

Baroclinic instability term

Assuming that within a volume element the density is constant one can write:

$$\frac{d\rho}{dt} = 0 \ , \tag{21}$$

Multiply (21) with ρ', keep the vertical velocity w negligible, let $u = \overline{u} + u'$, $v = \overline{v} + v'$, and take the time mean:

$$\overline{\frac{d}{dt}(\frac{1}{2} \cdot \rho'^2)} + \overline{\rho' \cdot u'} \cdot \frac{\partial \overline{\rho}}{\partial x} + \overline{\rho' \cdot v'} \cdot \frac{\partial \overline{\rho}}{\partial y} = 0 \ , \tag{22}$$

Multiplying (22) with $\frac{g}{\frac{d\tilde{\rho}}{dz}}$ and integrating over a volume V gives:

$$\frac{d}{dt}(EPE) = g \cdot \int\int\int \frac{\overline{u' \cdot \rho'} \cdot \frac{\partial \overline{\rho}}{\partial x} + \overline{v' \cdot \rho'} \cdot \frac{\partial \overline{\rho}}{\partial y}}{\frac{d\tilde{\rho}}{dz}} \, \mathrm{d}V \ ,$$

In the last calculation the fact that $\tilde{\rho}$ is independent of t, x and y and the vertical velocity w is negligible, is used, so that $\frac{d\tilde{\rho}}{dt} = 0$

Mean and kinetic energy

The kinetic energy per unit mass in a volume element V is given as:

$$KE = \int\int\int (u^2 + v^2) \, \mathrm{d}V \ , \tag{23}$$

Dividing all variables into a time-mean component and fluctuations ($a = \overline{a} + a'$) and taking the time mean, one can write:

$$KE = KEM + EKE \tag{24}$$

$$KEM = \int\int\int (\overline{u}^2 + \overline{v}^2) \, \mathrm{d}V \tag{25}$$

$$EKE = \int\int\int (u'^2 + v'^2) \, \mathrm{d}V \tag{26}$$

Barotropic instability term

By assuming that the flow is in geostrophic balance one can write:

$$\frac{du}{dt} = 0 \tag{27}$$

$$\frac{dv}{dt} = 0 \tag{28}$$

Writing all variables as a time-mean component and fluctuations, a = $\overline{a}$ + a', multiplying (27) with u' and (28) with v' and averaging one gets:

$$\overline{\frac{d}{dt}(\frac{1}{2} \cdot u'^2)} = -(\overline{u' \cdot u'} \cdot \frac{\partial \overline{u}}{\partial x} + \overline{u' \cdot v'} \cdot \frac{\partial \overline{u}}{\partial y}) \tag{29}$$

$$\overline{\frac{d}{dt}(\frac{1}{2} \cdot v'^2)} = -(\overline{v' \cdot v'} \cdot \frac{\partial \overline{v}}{\partial y} + \overline{u' \cdot v'} \cdot \frac{\partial \overline{v}}{\partial x}) \tag{30}$$

Adding (29) to (30) and integrating over a volume, gives (31), which gives the relation between the change in eddy kinetic energy and the work done by the Reynolds stresses.

$$\frac{d}{dt}(EKE) = -\int\int\int (\overline{u' \cdot u'} \cdot \frac{\partial \overline{u}}{\partial x} + \overline{u' \cdot v'} \cdot (\frac{\partial \overline{v}}{\partial x} + \frac{\partial \overline{u}}{\partial y}) + \overline{v' \cdot v'} \cdot \frac{\partial \overline{v}}{\partial y})\, \mathrm{d}V\ , \tag{31}$$

B Self induced motion

Westward translation due to β

In an open ocean the β force will accelerate a symmetric eddy in the meridional direction. The Coriolis force always act perpendicular to the motion, which after a certain time gives a meridional balance between the Coriolis and the β force, and thereby a zonal translation for the vortex. From Nof (1981) the β induced zonal velocity is given as:

$$C = -\beta \int\int \Psi \, \mathrm{d}x \, \mathrm{d}y \Big/ f_0 \int\int h \, \mathrm{d}x \, \mathrm{d}y \ , \tag{32}$$

Ψ is the stream function: $\frac{\partial \Psi}{\partial x} = v \cdot h$, $\frac{\partial \Psi}{\partial y} = -u \cdot h$. h is the eddy depth. For Equation (32) to be valid, $h \ll H$, where H is the total depth. This is not the case for the eddies in the Mozambique Channel, which leads to modification of Equation (32).

β force

Since the Coriolis force increases in magnitude away from the equator, a meso-scale symmetric vortex will gain a net Coriolis force either northwards or southwards. From Nof (1999) the Beta Force is given as:

$$\text{Beta Force} \qquad = \qquad \beta \int\int \Psi \, \mathrm{d}S \tag{33}$$

Ψ is again the stream function and S is the vortex area.

Rocket effect

Due to the β induced westward drift eddies are pushed towards solid walls (coastlines). Fluid can not penetrate these wall, so there will be a leakage. For anticyclonic vortices the leakage is northward. To conserve momentum, the remaining eddy will move along the coast the opposite direction of the leaked fluid. Anticyclones near a western wall move southwards.

Image effect

For a detailed description of the image effect, see Kundu and Cohen (2005).

1) Vortex flows can be given as:
solid body rotation $\quad u_\theta = \frac{1}{2} \cdot \omega \cdot r$,
irrotational vortex $\quad u_\theta = \frac{\Gamma}{2 \cdot \pi \cdot r}$,

where u_θ is the swirl velocity, ω the vorticity and Γ is the circulation.

2) In an irrotational vortex the only vortex line in the flow field is the axis of the vortex. In a solid body rotation, all lines perpendicular to the plane of flow are vortex lines.

3) Kelvin's Circulation Theorem
In an inviscid, barotropic flow with conservative body forces, the circulation around a closed curve moving with the fluid remains constant with time:
$\frac{d\Gamma}{dt} = 0$

4) Helmholtz Vortex Theorem
Vortex lines move with the fluid

5) Consider two vortices with opposite circulation placed a distance h from each other, as seen in Figure 30. Velocity at point 2 due to vortex Γ_1 is $u_\theta = \frac{\Gamma_1}{2 \cdot \pi \cdot h}$ northward. Since circulation Γ_2 is considered to be a point, the circulation must according to Kelvin's circulation theorem follow the point northwards.

6) Image effect
As there can be no flow into a solid wall, the flow will be reflected. The wall can then be eliminated and replaced by a vortex of equal strength and opposite circulation like in figure 30.

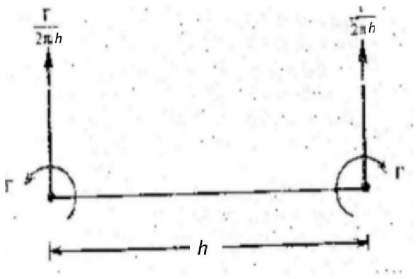

Figure 30: *Interaction of line vortices of opposite spin, but of the same magnitude. Here* Γ *refers to the magnitude of the circulation. The figure is from Kundu and Cohen (2005)*

C β-Induced Coastal Trapping of a Baroclinic Eddy

From Figure 12 and 13 it is seen that the swirl velocity of anticyclonic eddies in the Mozambique Channel can be written as:

$$v = \frac{4 \cdot v(\frac{r_0}{2})}{r_0} \cdot r \cdot (\frac{r}{r_0} - 1). \tag{34}$$

For an exact balance between the equatorward directed motion due to the β force and the advection by the southward background flow in the Mozambique Channel, the velocity of the background flow must be given as (Bowman, 1985):

$$U = \beta \cdot f_0 \cdot R_d^2 \cdot [0.285 + 0.918 \cdot (R_d/r_0)^2] \cdot \frac{sin(\alpha)}{3 \cdot K}\ , \tag{35}$$

where f_0 is the Coriolis parameter at a given location, β is the meridional gradient of f_0, R_d is the internal Rossby radius equal to $\frac{\sqrt{(g' \cdot h)}}{f_0}$ where g' is the reduced gravity ($g' = \frac{\rho_2 - \rho_1}{\rho_2} \cdot g$) and h is the eddy depth. K is a linearized bottom friction coefficient associated with the background flow and α is the inclination of the coastline (measured clockwise with respect to the east-west direction).

At 21 °S $f_0 = -5.2 \cdot 10^{-5} s^{-1}$, $\beta = 2.1 \cdot 10^{-11} m^{-1} s^{-1}$ and α =145 °. The modeled eddies have a radius between 100 km and 200 km (Fig. 10 and 11). In the upper 1500 m depth the density of the eddy center is lower than the water it is embedded in (Fig. 31). $\sqrt{(g' \cdot h)}$ has been calculated by subtracting the mean density of the eddy center (eddy 1) in the upper 1500 m depth from the mean density of the surrounding water in the upper 1500 m depth. From Matlab calculations R_d is then found to be equal to 37 km. The only unknown variable is K. The value used by Bowman (1985) in his calculation for the East Cape Current ($2 \cdot 10^{-6}$) has been chosen.

With these values U is found to be approximately 5 $\frac{\text{cm}}{\text{s}}$.

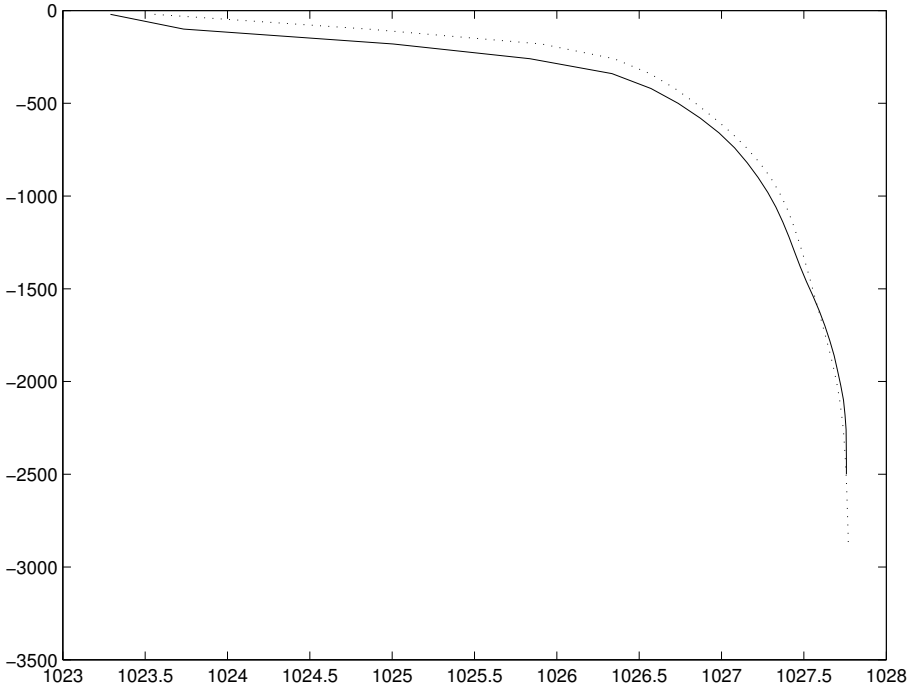

Figure 31: *Density of the center of eddy 1 (solid) and density of the water surrounding eddy 1 (dotted).*

D Condition for baroclinic instability

Potential vorticity $\overline{q}$ is from the quasi geostrophic equations given as (Cushman-Roisin, 1994):

$$\overline{q} = \frac{\partial^2 \overline{\Psi}}{\partial y^2} + \frac{f_0^2}{N^2} \cdot \frac{\partial^2 \overline{\Psi}}{\partial z^2} + \beta_0 \cdot y \ , \tag{36}$$

where Ψ is the stream function of the basic flow ($\frac{\partial \Psi}{\partial y} = U(y,z)$), N is the stratification frequency ($N^2 = -\frac{g}{\rho_0} \cdot \frac{d\overline{\rho}}{dz}$) and f_0 is the Coriolis parameter. A necessary condition for baroclinic instability, as described in Section 4.6, is that $\frac{\partial \overline{q}}{\partial y}$ changes sign somewhere in a two dimensional vertical section of the zonal current. From Equation (36) $\frac{\partial q}{\partial y}$ can be written:

$$\frac{\partial q}{\partial y} = -\frac{\partial^2 U}{\partial y^2} + \beta + \frac{f_0^2}{N^2} \cdot \frac{\partial}{\partial z}(\frac{\partial U}{\partial z}) \ , \tag{37}$$

$\frac{\partial U}{\partial z}$ can be found from the equations of motion, which for a zonal current in geostrophic balance is given as:

$$f_0 \cdot U = -\frac{1}{\rho} \cdot \frac{\partial p}{\partial y} \ , \tag{38}$$

where p is the pressure. Further, hydrostatic approximations is given as:

$$\frac{\partial p}{\partial z} = -\rho \cdot g \ , \tag{39}$$

where g is acceleration due to gravity.

Along density surfaces, variations of density is zero, which gives the following relations:

$$\Delta\rho = \frac{\partial \rho}{\partial z} \cdot \Delta z + \frac{\partial \rho}{\partial y} \cdot \Delta y = 0 \ , \tag{40}$$

Equation (40) $\rightarrow$:

$$\frac{\Delta z}{\Delta y}|_{\rho = constant} = -\frac{\partial \rho}{\partial y} \Big/ \frac{\partial \rho}{\partial z} \ , \tag{41}$$

From 39:

$$\frac{\Delta z}{\Delta y}|_{\rho = constant} = \frac{\partial}{\partial y}(\frac{1}{g} \cdot \frac{\partial p}{\partial z}) \Big/ \frac{\partial \rho}{\partial z} \ , \tag{42}$$

From 38:

$$\frac{\Delta z}{\Delta y}|_{\rho = constant} = -\frac{\partial}{\partial z}(\frac{\rho \cdot f_0 \cdot U}{g}) \Big/ \frac{\partial \rho}{\partial z} \sim f_0 \cdot \frac{\partial U}{\partial z} \Big/ N^2 \ , \tag{43}$$

In the last calculation the fact that $\frac{\partial U}{\partial z} \cdot \rho \gg \frac{\partial \rho}{\partial z} \cdot U$ has been used. It then follows that $\frac{\partial \overline{q}}{\partial y}$ can be written:

$$\frac{\partial \overline{q}}{\partial y} = \beta - \frac{\partial^2 U}{\partial y^2} - f_0 \cdot \frac{\Delta z}{\Delta y}|_{\rho = constant} \ , \tag{44}$$

References

AVISO (2006), 'ftp://ftp.cls.fr/pub/oceano/aviso/.'.

Bennet, A. F. & Kloeden, P. E. (1978), 'Boundary conditions for limited-area forecasts', *J. Atmos. Sci.* **35**, 990–996.

Biastoch, A. & Krauss, W. (1999), 'The role of mesoscale eddies in the source regions of the Agulhas Current', *J. Phys. Oceanogr.* **29**, 2303–2317.

Böning, C. W. & Büdich, R. G. (1992), 'Eddy dynamics in a primitive equation model: Sensitivity to horizontal resolution and friction', *J. Phys. Oceanogr.* **22**, 361–381.

Bowman, M. J. (1985), 'On the beta-induced coastal trapping of a baroclinic eddy', *J. Phys. Oceanogr.* **15**, 817–822.

Cushman-Roisin, B. (1994), 'Introduction to geophysical dynamics', *Prentice-Hall, Inc* .

De Ruijter, W. P. M., Ridderinkhof, H., Lutjeharms, J. R. E., Schouten, M. W. & Veth, C. (2002), 'Observations of the flow in the Mozambique Channel', *Geophys. Res. Lett.* **29**, 10.1029/2001GLO13714.

DiMarco, S., Chapman, P., Nowlin, W. D., Hacker, P., Donohue, K., Luther, M., Johnson, G. C. & Toole, J. (2002), 'Volume transports and property distributions of the Mozambique Channel', *Deep-Sea Res.* **49**, 1481–1511.

Gill, A. E. (1982), 'Atmosphere-ocean dynamics', *Academic Press, Inc* .

Gordon, A. (1986), 'Interocean exchange of thermocline water', *J. Geophys. Res.* **91**, 5037–5046.

Kalnay, E., Kanamitsu, M., Kistler, R., Collins, W., Deaven, D., Gandin, L., Iredell, M., Saha, S., White, G., Woollen, J., Zhu, Y., Chelliah, M., Ebisuzaki, W., Higgins, W., Janowiak, J., Mo, K. C., Wang, C., Leetma, A., Reynolds, R., Jenne, R. & Joseph, D. (1996), 'The NCEP/NCAR 40-year reanalyses project', *Bull. Am. Met. Soc.* **77**, 437–441.

Kundu, P. K. & Cohen, I. M. (2005), 'Fluid Mechanics', *Academic press Inc* .

Lutjeharms, J. R. E. (2005), 'The Coastal Oceans of South-Eastern Africa', *The Sea* **14b**.

Lutjeharms, J. R. E., Cooper, J. & Roberts, M. (2000a), 'Upwelling at the inshore edge of the Agulhas Current', *Cont. Shelf Res.* **20**, 737–761.

Lutjeharms, J. R. E., Wedepohl, P. M. & Meeuwis, J. M. (2000b), 'On the surface drift of the East Madagascar and the Mozambique Currents', *S. Afr. J. Sci.* **96**, 141–147.

Marchesialleo, P., McWilliams, J. C. & Shchepetkin, A. (2001), 'Open boundary conditions for long term integration of regional oceanic models', *Ocean Modelling* **3**, 1–20.

Matsuura, T. & Kamachi, M. (1993), 'The Evolution of Isolated Vortices Interacted with Steep Slope', *Journal of Oceanography* **49**, 317–352.

Nof, D. (1981), 'On the beta-induced movement of isolated baroclinic eddies', *J. Phys. Oceanogr.* **11**, 1662–1672.

Nof, D. (1999), 'Strange encounters of eddies with walls', *J. Mar. Res.* **57**, 739–761.

Oort, A. H., Ascher, S. C., Levitus, S. & Peixoto, J. P. (1989), 'New estimates of the available potential energy in the world ocean', *J. Geophys. Res.* **94**, 3187–3200.

Pedlosky, J. (1987), 'Geophysical Fluid Dynamics', *Springer-Verlag* .

Pedlosky, J. & Spall, M. (1999), 'Rossby normal modes in basin barriers', *J. Phys. Oceanogr.* **29**, 2332–2349.

Quadfasel, D. R. & Swallow, J. C. (1986), 'Evidence for 50-day period planetary waves in the South Equatorial current of the Indian Ocean', *Deep-Sea Res.* **33**, 1307–1312.

remss (2006), 'http://www.remss.com/.'.

Ridderinkhof, H. & de Ruijter, W. P. M. (2003), 'Moored current observations in the Mozambique Channel', *Deep-Sea Res.* **50**, 1933–1955.

Ridderinkhof, H., Lutjeharms, J. R. E. & de Ruijter, W. P. M. (2001), 'A research cruise to investigate the Mozambique Current', *S. Afr. J. Sci.* **97**, 461–464.

Roed, L. P. & Fossum, I. (2002), 'Mean and eddy motion in the Skagerrak/northern North Sea: insight from a numerical model', *Ocean Dynamics* **54**, 197–220.

Sæ tre, R. (1985), 'Surface currents in the Mozambique Channel', *Deep-Sea Res.* **32**, 1457–1467.

Schott, F., Fieux, M., Kindle, J., Swallow, J. & Zantopp, R. (1988), 'The boundary currents east to Madagascar 2. Direct measurements and model comparisons', *J. Geophys. Res.* **93**, 4963–4974.

Schouten, M. W., de Ruijter, W. P. M., van Leeuwen, P. & Ridderinkhof, H. (2003), 'Eddies and variability in the Mozambique Channel', *Deep-Sea Res.* **50**, 1987–2003.

Shi, C. & Nof, D. (1994), 'The destruction of lenses and generation of woodons', *J. Phys. Oceanogr.* **24**, 1120–1136.

Song, Y. & Haidvogel, D. (1994), 'A semi-implicit ocean circulation model using a generalized topography-following coordinate system', *J. Comput Phys.* **115**, 228–244.

Stramma, L. & Lutjeharms, J. R. E. (1997), 'The flow field of the subtropical gyre of the South Indian Ocean', *J. Geophys. Res.* **102**, 5513–5530.

Strauss, W. A. (1992), 'Partial differential equations: An introduction', *John Wiley and sons, Inc* .

Svendsen, E., Sæ tre, R. & Mork, M. (1991), 'Features of the northern North Sea circulation', *Cont. Shelf Res.* **11**, 492–508.

Weijer, W., de Ruijter, W. P. M., Sterl, A. & Drijfhout, S. (2002), 'Response of the Atlantic overturning to South Atlantic sources of buoyancy', *Global and Planetary Change* **91**, 5037–5046.

Wright, D. G. (1987), 'Baroclinic instability: Energy transfer and the role of potential vorticity conservation', *Atmos-Ocean* **25**, 225–241.

Zavala, L., Graef, F. & Pavia, E. G. (1998), 'Collisions of anticyclonic, lens-like eddies with a meridional western boundary', *J. Geophys. Res.* **103**, 24881–24890.